The Essex Echo: Unification - track I

A recent and enthusiastic meeting of the British Section of the Audio Engineering Society (AES), via a shows of hands, expressed a consensus that, in principle, amplifiers do exhibit perceptual differences in performance when auditioned under favourable conditions. The occasion was Martin Collom's lecture entitled "Amplifiers: Do they sound different?", when over 120 members gathered to experience a lecture integrated with discussion and audio demonstrations.

1985 has seen an emerging awareness that there are numerous error sources within an audio system that demand more detailed research, as it is evident that they contribute directly to perceptual sonic differences. Over the next four editions of the Essex Echo, I am going to explore several facets of error mechanisms with a particular emphasis on the loudspeaker-interconnect interface, capacitors and inductors.

Our thesis will attempt a unification of these interactive error processes by both presenting and applying a detailed study of transmission line systems and supporting electromagnetic theory. This avenue of research stems from the observation that several linear error mechanisms result directly from wave propagation in the acoustical, mechanical and electrical domains that, in turn, are linked by mutual interdependence. It will be shown that, in essence, a single mathematical model is applicable directly to both interconnects and capacitors and when compounded with our notion of the transfer-error function (1,2) a powerful conceptual model of error structure emerges. In part, the presentation will be rigorous though interlaced with illustrative discussion; I hope the mathematical detail will provide a more comprehensive background to allow a greater appreciation of the theory and thus gain in tutorial value.

In the present series, we will err on the side of caution and attempt to create a model only for the linear and continuous set of systems; I will leave more radical investigation for a later date as my personal conviction suggests that low-level threshold phenomena, conductor granularity and directionality set bounds upon the ultimate transparency of an audio system, factors that I collectively term 'Fuzzy Distortions'.

Applying a logical strategy to the subject of interconnects, there appear to be three areas for research:

(i) Low-level systems, where signal levels fall to 10's nano volt, may well fall into the regime of Fuzzy Distortions.

(ii) Medium-level interconnects, where there is no significant signal power, may nonetheless introduce perceptual change, not so much by the interconnect directly but by the change the cable characteristics impose upon the electronics. Thus, when performing measurements, it may well prove constructive to look for a differential in the overall system transfer-error function when interconnects are changed.

(iii) High-level signals over the loudspeaker interconnect, where interconnects play a dominant role in establishing an error mechanism.

Those readers familiar with my earlier essays in HFN (1,2,3) will be aware that I have used the transfer-error function as a method of exposing the linear distortions exhibited within an audio system (in earlier articles I have used the term 'error function', though I now prefer the generic term 'transfer-error function'). This function has already been experimentally used by both John Curl (4,5) and, more recently, Martin Colloms (6) where Martin also presented a convincing public demonstration using music signals, during his AES lecture.

It is important to note that though a system may exhibit noise and non-linear distortion <80dB, that linear distortions (1,2,3) are orders of magnitude above this figure and often within a range 5 to 60dB below the primary signal. I personally advocate that much of the non-ideality exhibited by audio equipment is more accurately specified by linear distortion. In practice, our measurement techniques do not always address this aspect of distortion though recent research, for example, on Cepstrum analysis (8,9) offers a welcome advancement. Also, at a more philosophical level, engineers often fail to appreciate that ultimately all objective measurements are subjective: they require interpretations as to their sonic character, a sequence of numbers is not by itself sufficient unless of vanishing magnitude, though this is

never achieved for complete systems. Thus even though the transfer-error function is capable of an exact representation of linear distortion, it is the subjective interpretation of the resulting error that is the final arbiter.

My motivation for composing a further treatise on interconnects and capacitors has resulted from four disparate experiences during 1985. Two have already been adequately reviewed, namely John Curl's error test (4) during my visit to San Francisco in May and, later, Martin's AES lecture on December 10.

The third factor is due to Dennis Morecroft of DNM who walked into my office at Essex University and placed a number of electrolytic capacitors on my desk, claiming they were of modified construction, where the conductive surfaces had been partially slit, as Dennis explained, to reduce circulating currents within the plates. He claims that this technique of implanted alignment to the distribution of current, lowers the inductive component and results in an improved high frequency performance. Dennis is an audio designer with exceptional intuition, and one learns to take notice of his work.

The final node in the network occurred during a recent visit to Paris where Peter Ainscough runs a high-end audio company called FAMCO (French American Company). Visiting Peter is always a rewarding experience, as he has immense enthuasism for his work and this occasion was to be no exception. On Friday evening, we drove into the suburbs of Paris to visit Yves Bernard Andre. It was on this cold Parisian evening that I was to experience, for me, a quantum step forward in audio reproduction. Yves has researched and developed every element of his system, no component or interconnect has been passed without careful audition as to sonic characteristic and directionality. To say this system was impressive is an understatement: the sound exhibited a dynamic and transparent quality that embeds a very convincing sense of realism, the very characteristics so often missing from reproduced music, that immediately informs the listener the sound is not live. This system further convinced me that the quest for dynamic and transient integrity (no compression of transients) is a fundamental

objective and when integrated with our notion of dimensionality (as initially proposed by J. Zelinger of Automation Sciences, and transparency (see Harry Pearson's recent essay (10)), we can only then begin to contemplate perfection.

Stanley Kelly recently related a story (see also (11)) to me during the HFN Annual Dinner (thanks for invite John, I liked the white suit!) of a very high quality professional reproduction system that was directly linked to the studio complex. The reproduction, however, although of high calibre, simply did not convey a sense of live music and this was an environment where such a objective could be expected. I would suggest at this point in time that this situation is rather typical, suggesting factors still not universally understood or appreciated. I anticipate the final steps in opening-up system transparency may upset some engineering sensitivities, but then as Martin proclaimed during discussion time at the AES "Failure to consider these factors will result in audio performance remaining trapped in the 1980s".

For me, 1985 will be remembered as an occasion for appreciating the work of designers from various countries, where I now feel I have a greater overall awareness of the objectives and ultimate capabilities of an audio system that transcends certain engineering dogma. I will, therefore, attempt to assimilate some of these notions by re-exploring the models upon which design principles are based. This quest commences in this current series.

The primal concept is that many error mechanisms are associated with wave propagation whether these are interconnects (3), large-area capacitors, loudspeaker diaphragms or loudspeaker enclosures (2,11). Recently there has been a trend to model interconnects and capacitors using multi-stage, lumped arrays of LRC components in an attempt to realise an improved match between system and model. This method, though useful, does not result in an exact model for arbitrary bandwidth and actually leads to far greater computational complexity due to multi-node analysis.

The approach we shall adopt is to use a distributive structure using the principles of transmission line theory (13). This allows,

for example, an accurate prediction of interconnect non-ideality when loaded by a high performance loudspeaker, such as the Celestion SL600 both within and beyond the audioband. The model can readily incorporate the internal conductor wave effects (3) giving rise to skin depth, where I will later show a loudspeaker interconnect to be a two-dimensional, distributive transmission line. Also, as a bonus, the final calculations are relatively straightforward and computationally efficient, even though the intermediate derivations are somewhat tortuous.

To commence our study, this first track will revise a typical loudspeaker model incorporating two drive units and a crossover with the aim of accurately predicting the loudspeaker impedance that will ultimately load the loudspeaker interconnect. This impedance is then used as a reference for comparative interconnect assessment.

Loudspeaker system impedance modelling

A typical loudspeaker, moving coil drive-unit construction is shown in Fig.1 where the principle system elements are the magnet, magnetic circuit, moving coil motor, diaphragm system and suspension.

The first objective is to make an estimate of the drive-unit impedance as seen at the voice-coil terminals, this impedance can then be interfaced with the crossover topology to allow a complete evaluation of the composite, input impedance.

The voice coil and magnet system act as a transformer between the mechanical and the electrical domains. Central to this transformation is the {Bl} product where, in general

$$\{Bl\}\,\hat{a} = \int_{C_v} \bar{B} \times d\bar{l}$$

$\hat{a}$ is a unit vector mutually at right angles to the plane containing the vectors $\bar{B}$ and $d\bar{l}$: it is directed along the axis of the voice coil

where, $\bar{B}$ is the magnetic flux density, $d\bar{l}$ an element of the voice coil and C_v a contour in space defined by the voice-coil path. In practice,

the product {Bl} is non-linear with the axial displacement of the voice coil and is a fundamental distortion mechanism. In this article, we will note its existence but assume linearity: {...} brackets are used to indicate an integration taken over the coil length where, in general $\overline{B}$ is non uniform.

There are two governing electromagnetic principles in the operation of the drive unit; these are the motor and generator effects, respectively, which are represented by the two relationships,

$$f = \{Bl\}\, i$$

note the {Bl} product in each case

$$e = \{Bl\}\, v$$

i , current in voice coil, ampere
f , total force on voice coil, newton
v , velocity of voice coil, metre/s
e , generator emf in speech coil, volt

The two equations enable a transformation from mechanical impedance Z_m to electrical impedance Z_e, where

$$\text{if, } Z_m = \frac{f}{v} \text{ , } Z_e = \frac{e}{i} \text{ , then } Z_e = \frac{\{Bl\}^2}{Z_m}$$

Since this series of articles is only indirectly concerned with drive-unit performance, we shall assume the diaphragm to operate in the piston region (i.e. all elements move as a single entity) whereby the mass of the coil, and diaphragm assembly can be lumped as a single mass M_m. Similarly, the suspension and enclosure volume is modelled as a linear compliance C_m. Also, when in motion, there is an acoustic air load on the diaphragm together with a resistive loss component when the suspension is flexed. Consequently, the classic series analogue equivalent circuit of the mechanical parameters can be represented as in Fig.2a (14), where velocity 'flows' through each component producing a resulting force: it is directly analogous to current and voltage, current → velocity, force → voltage. The analogy even includes a constant force generator, {Bl}i.

and then replay the error in stereo for subjective appraisal. This would enable both a subjective assessment of the error signal as well as an estimate of the stereo information. The same concept is applicable to John Curl's and Martin Colloms' capacitor error test. This method should become an integral technique within loudspeaker interconnect assessment and compares with my earlier suggestion (5) for auditioning loudspeaker enclosure errors.

I feel these observations to be important, as it is generally believed that the resolution of system errors are best observed in stereo where the impact upon transparency, dimensionality and dynamic and transient integrity is more apparent. A subjective monitoring environment must embody all the perceptual clues available for fine resolution to be achievable. Small differential channel errors in frequency response represent relatively large differential channel errors in transfer-error function. I have read with interest the recent letter by Dr Lesurf (9) who appears to agree with me in this area, I thank him for his comments.

Measurement of conductor internal loss wave (skin depth) in the time domain

As a final observation of skin depth phenomena and to substantiate my original claim (8) that the internal propagating fields, that are directed along the radius represent a lossy energy reservoir that time smear a small fraction of the applied signal, I will present some measurements and computer simulation of this phenomena. Note my claim that, for a conductor operating in a skin depth limited region ($\delta < Z$), is that the time dispersion is significant, though the error is at low level. I previously suggested (8), that if a tone burst of current was passed through a conductor, when the tone was switched off, the internal propagating loss wave would have to dissipate before the error voltage across the conductor was zero, as the loss wave is effectively temporary stored energy.

For the experiment, a multi-strand steel conductor of 2.6mm diameter was used. A thin heat shrink sleeve was placed over half its length and the cable then folded symmetrical to form a short circuit, parallel interconnect with minimal dielectric space between conductors. Finally, a larger heat shrink sleeve was placed over the whole cable to hold the conductors tightly together, again to minimise the enclosed area, by keeping the parallel conductors in close proximity.

The purpose of the construction was two-fold:

(i) steel being magnetic, the skin depth effects are exaggerated as δ is a function of μ (hence my dislike of steel pipes)

The composite equivalent circuit of Fig.3 is finally analysed by computer to obtain the magnitude and phase of the SL600 load impedance. In Fig.4, three traces are shown:

Trace 1 actual measured modulus of impedance of typical SL600

Trace 2 computer estimate of SL600 impedance ignoring pole-piece coupling

Trace 3 computer estimate of SL600 impedance including pole-piece coupling

Examining the traces reveals excellent agreement between measurement and computer results, where trace 2 illustrates the importance of including pole-piece coupling, especially close to a resonant mode.

The principle advantage of establishing a computer model of the SL600 is to enable a data file of both amplitude and phase to be embedded within the final transfer-error function analysis program. It also enables the effect of component tolerances and individual component sensitivities to be explored as part of a more general research.

Digression

As an aside, while debating the SL600 load impedance, it is clear from Fig.3 that the hf and lf crossover filter sections are independent, that is until a long interconnect between amplifier and loudspeaker is introduced. Fig.5 shows the individual impedance plots for the respective crossover sections, where the results reveal a less demanding load compared to the composite plot of Fig.3, trace 2. At Essex, we separated the filter sections of our SL600 and repositioned them in close proximity to the power amplifier, which achieved 5 principle advantages:

(i) reduction in composite interconnect transfer-error function

(ii) individual hf and lf interconnect structures can be optimised for their respective bands of operation, with a reduction of of current demand on each interconnect

(iii) enhancement in crossover earthing configuration

(iv) simple pseudo-active configuration feasible using separate power amplifiers for each filter section. This achieves a closer approximation to star earthing for each filter section and significantly reduces amplifier current demand both by eliminating input impedance interaction of the parallel filter sections and by separating hf and lf signal components

(v) almost complete elimination of crossover vibration as filters now external to loudspeaker enclosure

[These comments apply to most loudspeaker systems and do not suggest any principle failing of the SL600. The SL600 was selected here primarily on its very excellent subjective merit.]

The modification (iv) is particularly applicable for remote power amplifiers such as the Quad 405, where a dedicated stereo amplifier is used for each channel with the inputs simply paralleled, as both amplifiers require the same gain. Did I hear Peter Walker murmur that there is something in subjectivity after all! Thanks in particular are due to research students Paul Mills and Richard Bews for their enthusiastic (out of hours) pursuit of this modification, where the final system configuration is shown in Fig.5.

Conclusion

The main characteristics of the loudspeaker load impedance are now complete as a prelude to the more formal study of transmission line theory to be presented on later tracks in this series. The principle objective is to establish a model for interconnects that includes distributed inductance, capacitance and loss fields for non-granular conductors. This model when interfaced to a loudspeaker load will enable an exact prediction of the error mechanism both within and beyond the audio band, the latter being important for amplifier loading.

A second factor of interest is the characteristic impedance of an interconnect, where it will be shown that at audio frequencies this impedance is generally misrepresented and that the concept of cable

matching, as normally applied, is essentially a nonsense. Also, I am concerned by the figures often quoted for loop inductance; they do not always appear to agree with the basic theory.

At the commencement of track I, I intimated that the transmission line model would be extended to include capacitors, thus forming a more unified concept. Indeed, observations of the structure of large, electrolytic capacitors reveal plate dimensions in excess of 6m: the structure is an open-circuit transmission line with propagation in two dimensions; we will later attempt to relate this to Dennis Morecroft's claims on slit plates.

Our investigations are attempting to show that audio system evaluation often fails on two counts: first, the exactness of the designer's model may be flawed, and second, the accuracy and interpretation of measurements do not result in a precise specification due to poor measurement resolution and measurement noise.

The revolution now encompasses dimensionality, transparency and transient and dynamic integrity; they are the key to realism. There are at present several exciting technological developments on the horizon, using both optical and magnetic media. However, for me, their ultimate success will depend more on the elegance and precision of the analogue signal processing and interfacing: of such stuff dreams are made ...

To be continued ...

References:

1 M.J. Hawksford, 'The Essex Echo: on errors, low feedback and fuzzy distortion', HFN/RR, Vol.29, No.9, pp.37-41, September 1984

2 M.J. Hawksford, 'The Essex Echo: Reflexions', HFN/RR, Vol.30, No.12, pp.35-40, December 1985

3 M.J. Hawksford, 'The Essex Echo: Maxwellian theory and interconnect memories', HFN/RR, Vol.30, No.8, pp.27-33, August 1985

4 J. Curl, 'About the "sound" of capacitors', Letter to Editor, HFN/RR, Vol.30, No.8, p.15, August 1985

5 J. Curl and W. Jung, 'A real-time signal test for capacitor quality', Audio Amateur Magazine, 4/1985, pp.22-24, 1985

6 M. Colloms, 'Capacity to change', HFN/RR, Vol.30, No.12, pp.53-57, December 1985

7 D. Preis, 'Linear Distortion', JAES, Vol.24, No.5, pp.346-367, June 1976

8 R.B. Randall, J. Hee, 'Cepstrum Analysis', Brüel and Kjaer Technical Review, No.3, pp.3-40, 1981

9 P.D. Bauman, S.P. Lipshitz, T.C. Scott, J. Vanderkooy, 'Cepstral Techniques for Transducer Measurement', 76th Convention of the AES preprint 2172 (B-3), October 1984

10 H. Pearson, 'The second American audio revolution', HFN/RR, Vol.31, No.1, pp.37-39, January 1986

11 S. Kelly, 'Loudspeaker logistics', HFN/RR, Vol.30, No.12, pp.61-65, December 1985

12 J.M. Kates, 'Loudspeaker cabinet reflection effects', JAES, Vol.27, No.5, pp.338-350, May 1979

13 F.R. Connor, Wave Transmission, Edward Arnold (Publishers) Ltd., ISBN 0 7131 3278 7, 1972

14 H.F. Olsen. Acoustical Engineering, D. Van Nostrand Company, Inc. Library of Congress Catalog Card 57-8143, pp.152-157, 1967

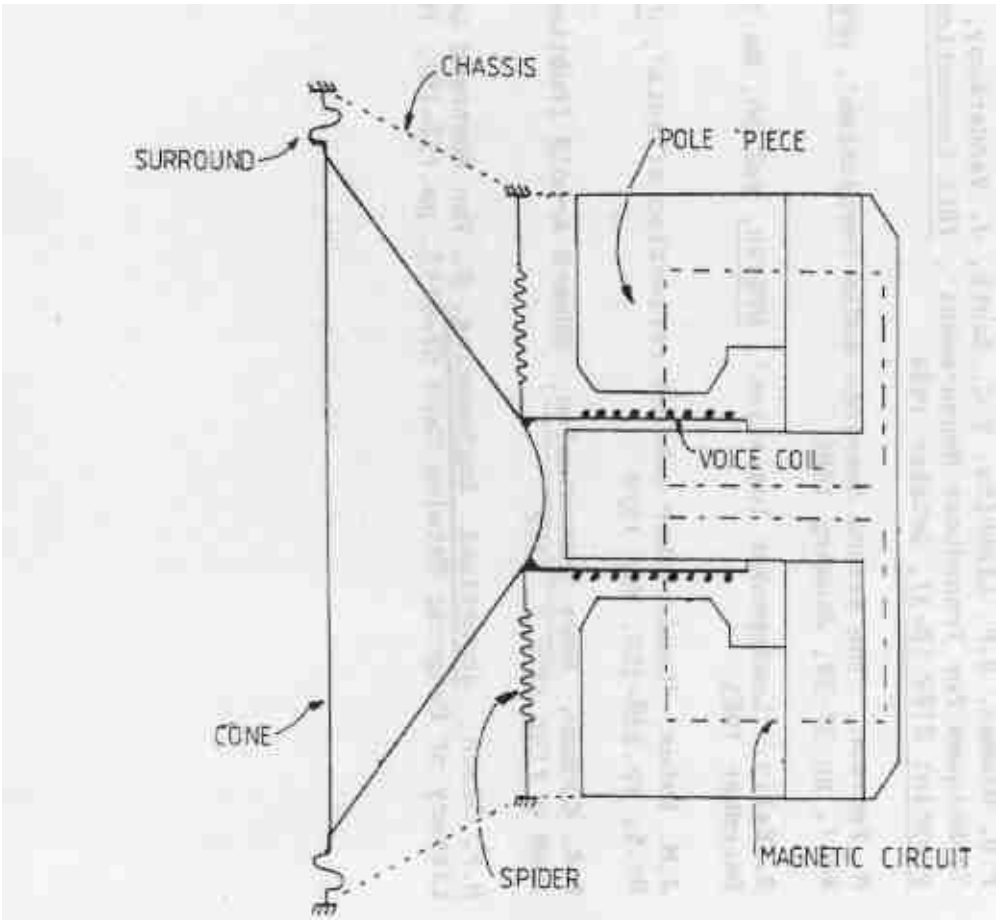

Fig.1 Moving-coil drive unit schematic

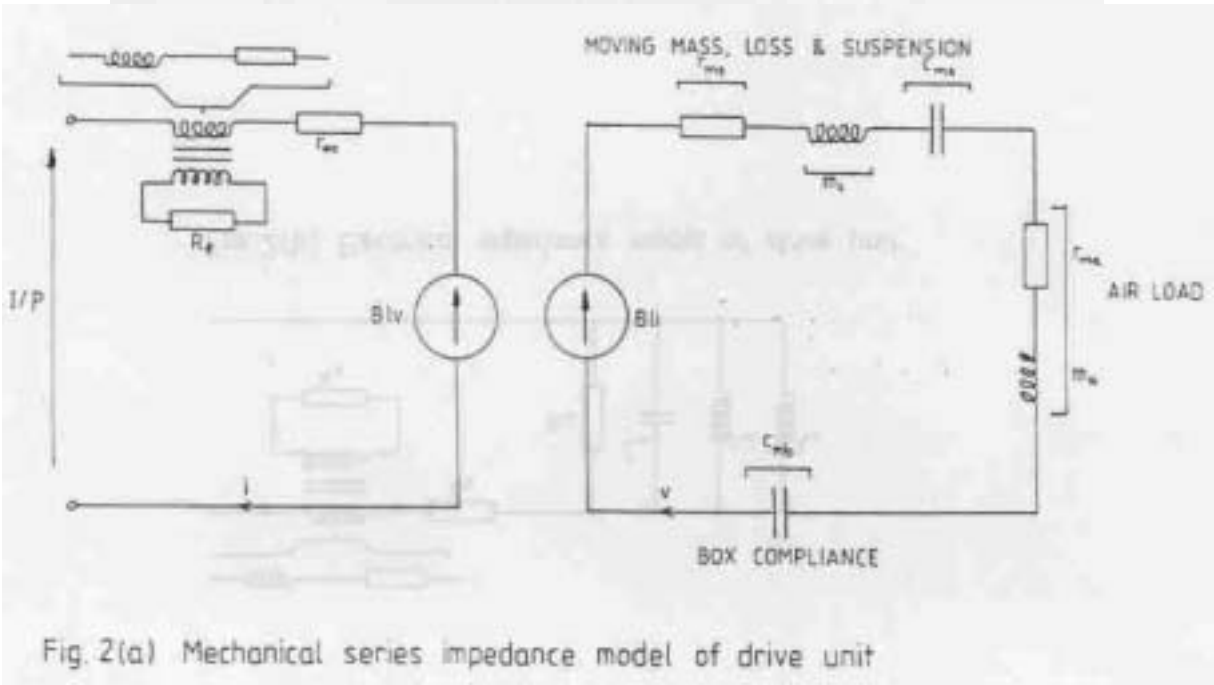

Fig. 2(a) Mechanical series impedance model of drive unit

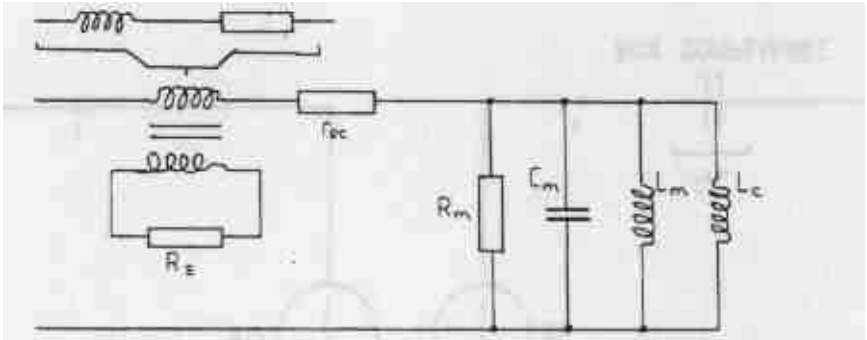

Fig. 2(b) Electrical impedance model of drive unit

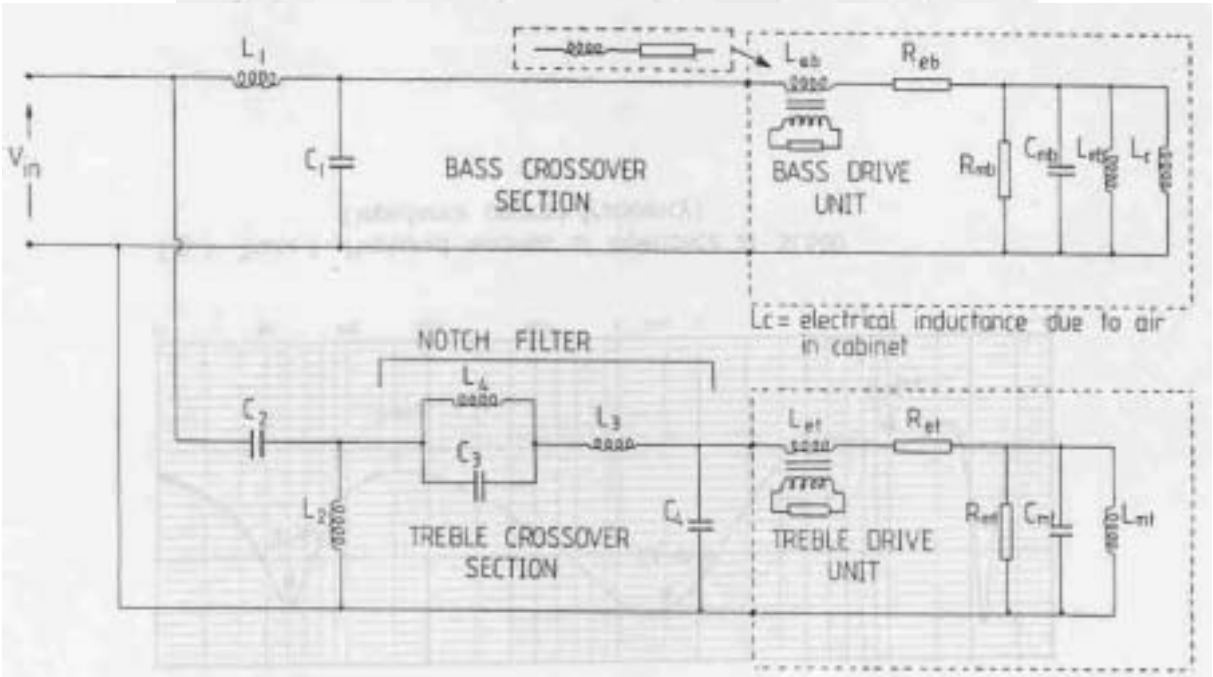

Fig.3 Loudspeaker system crossover and drive unit electrical model (Celestion SL600)

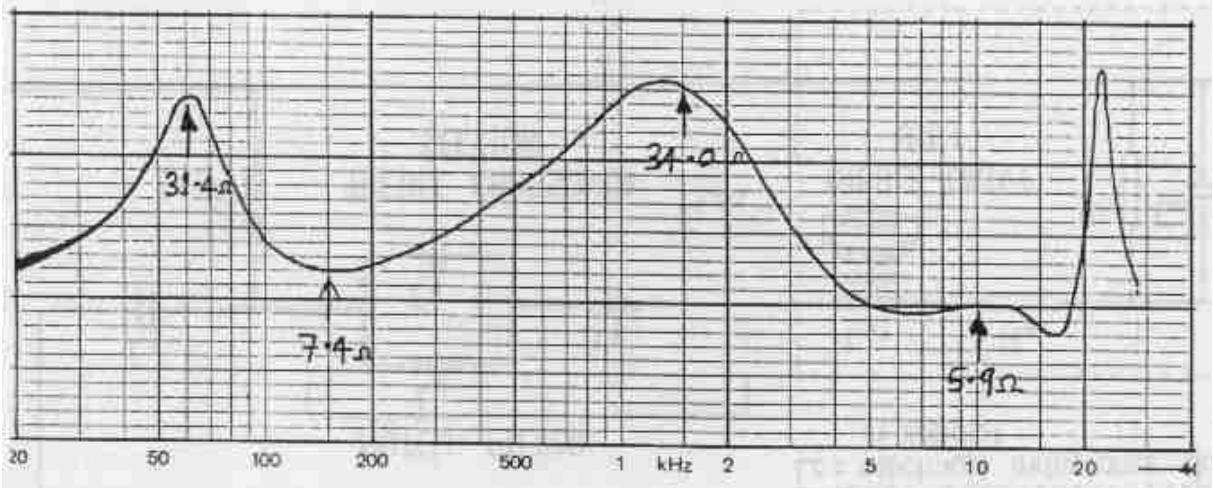

Fig. 4 Trace 1: Measured modulus of impedance of SL600 (impedance against frequency)

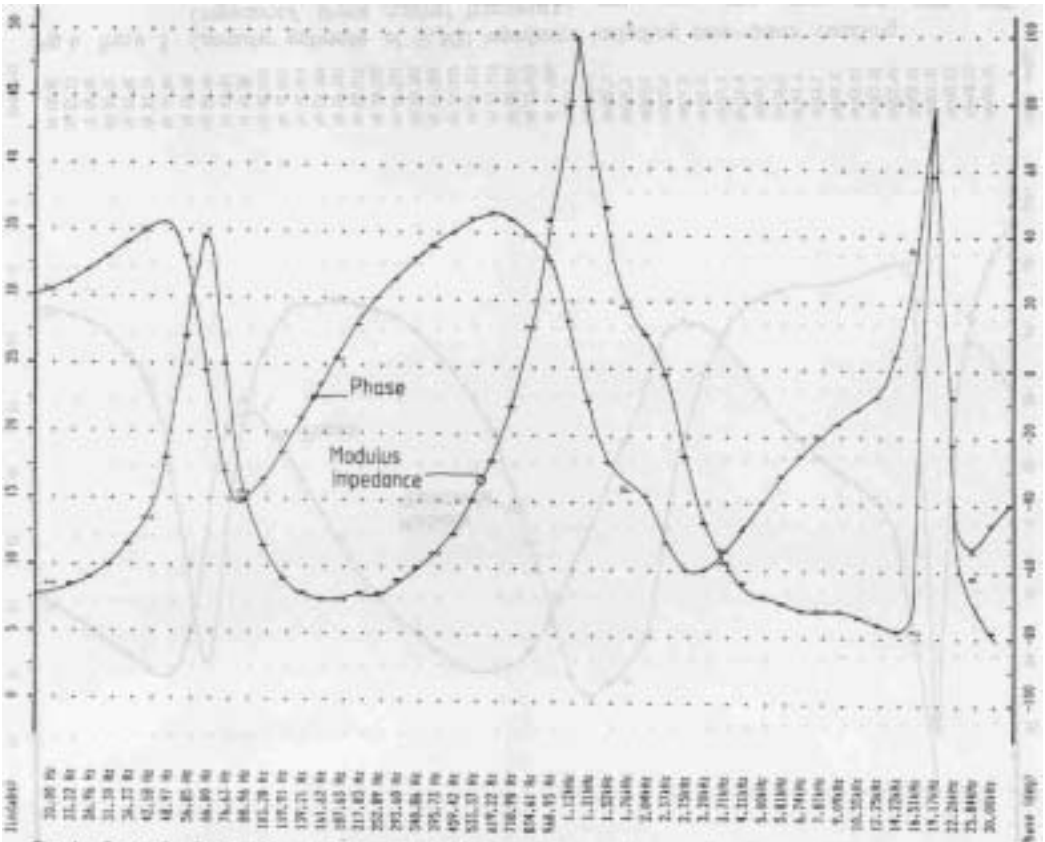

Fig 4 Trace 2: Computer estimate of SL600 impedance with no pole-piece coupling (impedance, phase against frequency)

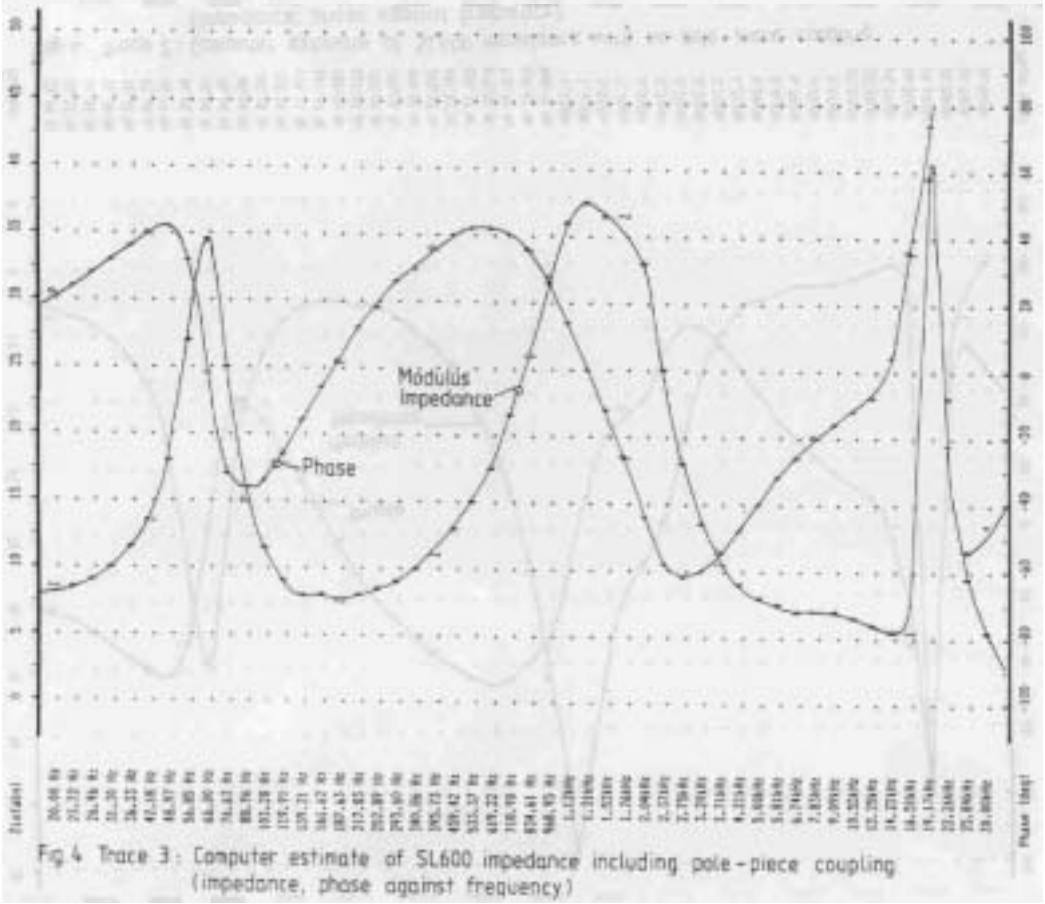

Fig 4 Trace 3: Computer estimate of SL600 impedance including pole-piece coupling (impedance, phase against frequency)

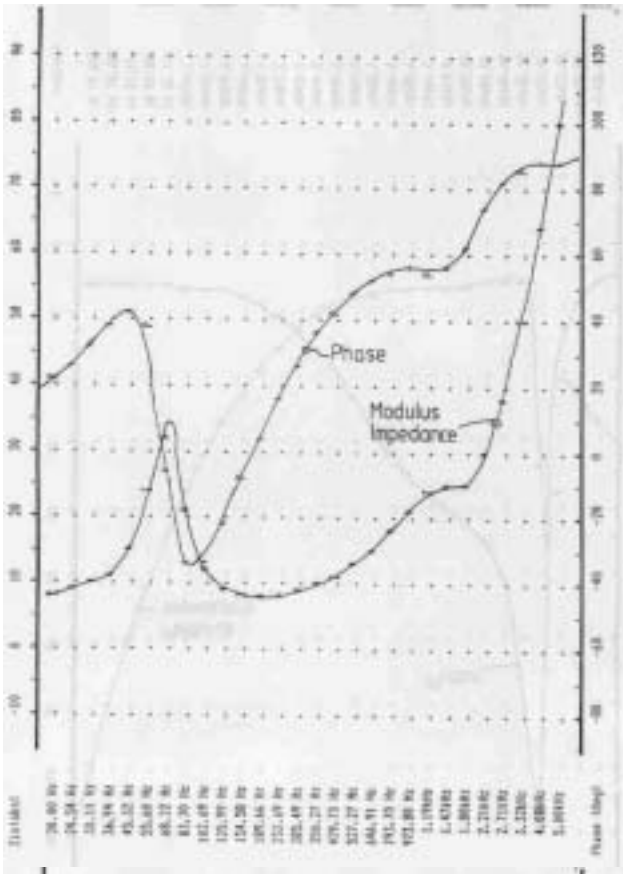

Fig 5(a) Bass crossover section impedance (impedance, phase against frequency)

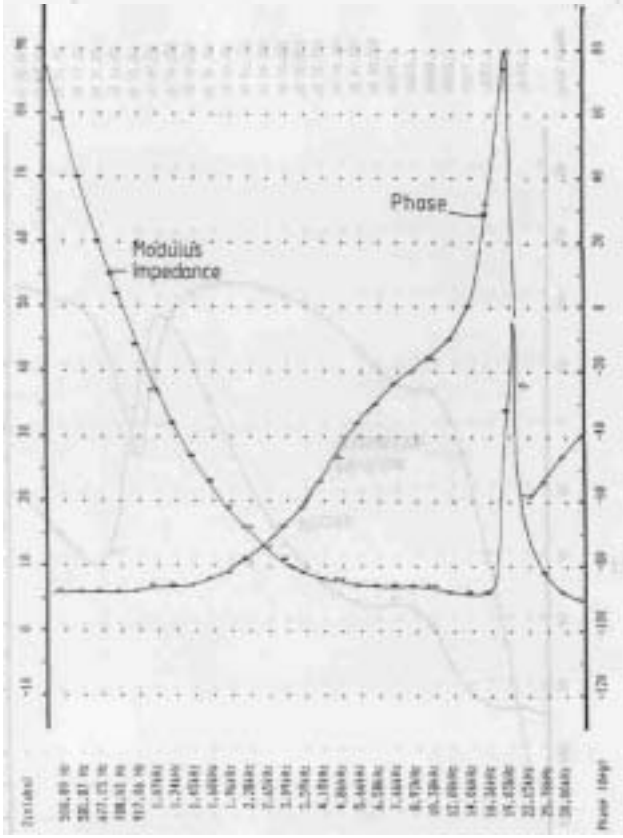

Fig 5(b) Treble crossover section impedance (impedance, phase against frequency)

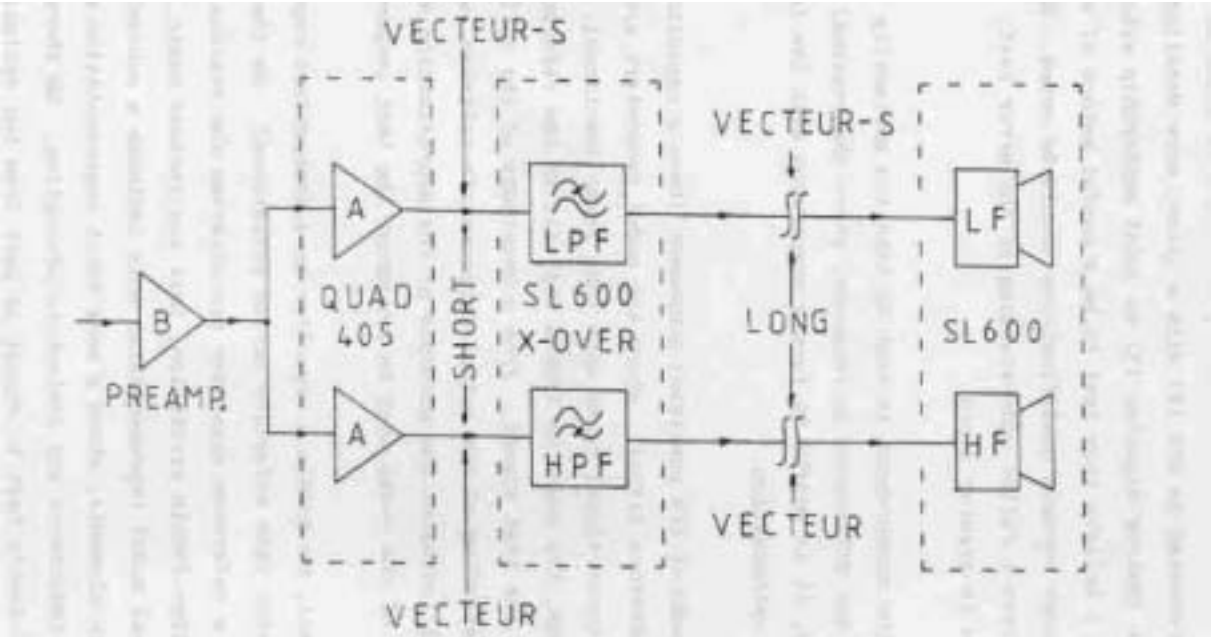

Fig 5C Basic structure of pseudo active system based for illustration on Quad 405, Celestion SL600, and Vecteur S and standard Vecteur interconnects.

APPENDIX

Comments on Measurement of Capacitor Errors using Difference Techniques

The test circuit that was introduced by John Curl is shown in Fig.A1 and was originally presented in HFN (4) with a later, more detailed, discussion, in the Audio Amateur Magazine (5) in joint authorship with W. Jung. In principle, I believe this test to be a useful method of exposing capacitor errors, though certain qualifications should be noted. Hence, in order that we achieve a fuller understanding of the error test, let us explore its operation in greater depth.

The essence of the measurement is that we take two notionally identical circuits and extract the difference in response, where the residual represent non-ideality. Indeed, it is useful to form a comparison with the techniques employed in computer optimisation.

Essentially, a model of the non-ideal component (here a capacitor) is compared against a reference circuit, where the model parameters are adjusted to achieve a minimum error signal based upon some error functional. When the residual is minimum, the model is then a best fit to the reference within the context of the test signal. From a knowledge of the optimised model, a better understanding of the actual component is achieved, while measuring the residual indicates the accuracy of the approximation and thus the completeness of the model used to represent the test component.

In John Curl's test, he models a capacitor as a theoretical capacitor in series with a resistor (the effective series resistance). He then compares this against a reference capacitor and observes the residual error for a range of time-domain excitation, that can include music. In principle, the non-ideal model representation only includes a sub-set of the capacitor parasitic elements, where a more exact representation would include, for example, inductance and dielectric absorption. We therefore expect the residual of John's test to result in part from the exclusion of these parasitics.

Continued...

Comments on Measurement of Capacitor Errors ... (continued)

The central problem in performing the error test is knowing when the variables have been optimised in a global sense and not just locally optimised either to a local minima or to a specific test signal. The latter point is particularly important when the number of variables are small (local minima are a problem as the number of variables in the optimisation proliferate). The danger is that we optimise the circuit to a specific test signal, e.g. a single sine wave or a single rectangular pulse, otherwise the observed distortion is misleading. For audio, I would suggest that band-limited, white noise is applied to the test circuit and the variables optimised to achieve a minimum rms error signal; the high-pass, frequency selectivity of the error signal also needs to be accounted in the operation.

Assume we have a reference capacitor C_o with an effective series resistance r_o which is compared against a test capacitor C_1 with effective resistance r_1. The test circuit is shown in Fig. A1, where the difference amplifier gain is A and the non-inverting and inverting inputs have small gain errors $(1 + \alpha)$, $(1 - \alpha)$ respectively ($\alpha \ll 1$).

Let, $T_o = R_o C_o$ $\tau_o = r_o C_o$

$T_1 = R_1 C_1$ $\tau_1 = r_1 C_1$

Analysing the transfer function $\frac{V_o}{V_1}$ of the error circuit,

$$\frac{V_o}{V_1} = j\omega A \left[\frac{\{(T_o - T_1) + \alpha(T_o + T_1)\} + j\omega\{(T_o\tau_1 - T_1\tau_o) + \alpha(2T_oT_1 + T_o\tau_1 + T_1\tau_o)\}}{(1 + j\omega(T_o + \tau_o))(1 + j\omega(T_1 + \tau_1))} \right]$$

{Note the sensitivity to α as $T_1 \to T_o$ and $\tau_1 \to \tau_o$}

or for the case where $\alpha = 0$,

$$\left.\frac{V_o}{V_1}\right|_{\alpha=0} = j\omega A \left[\frac{(T_o - T_1) + j\omega(T_o\tau_1 - T_1\tau_o)}{(1 + j\omega(T_o + \tau_o))(1 + j\omega(T_1 + \tau_1))} \right]$$

Continued...

Balance is achieved where $T_o = T_1$ and $\tau_o = \tau_1$ (for $a = 0$) i.e. both real and imaginary parts must be zero. If both the test and the reference capacitor can be modelled by a single parasitic resistor in series with a theoretic capacitor, then a broadband null is attainable. However, if the basic model is incomplete, the error circuit response cannot be simultaneously nulled for all frequency as the optimum alignment is frequency dependant.

To illustrate this observation, consider an example where both the reference and test capacitors have parasitic series inductances L_o, L_1 henry, such that $\omega_{no} = (L_o C_o)^{-0.5}$ and $\omega_{n1} = (L_1 C_1)^{-0.5}$ respectively.

Repeating the error analysis of the test circuit now reveals,

$$\frac{V_o}{V_1} \approx -j\omega A \left[\frac{\{T_1 (1-(\frac{\omega}{\omega_{n0}})^2) - T_0 (1-(\frac{\omega}{\omega_{n1}})^2)\} + j\omega (T_1 \tau_0 - T_0 \tau_1)}{(1 + j\omega (T_0 + \tau_0) + (j\frac{\omega}{\omega_{n0}})^2)(1 + j\omega(T_1 + \tau_1) + (j\frac{\omega}{\omega_{n1}})^2)} \right]$$

Since the error test circuit of Fig. A1 does not include a balance mechanism for the inductive parasitics, then the expression reveals that a broadband null is unattainable for $\omega_{no} \neq \omega_{n1}$ as the imaginary term is frequency dependant. Consequently, for this example, John's test can only be balanced at a single frequency, though that frequency can be selected at random. A similar argument can be presented for the parasitic elements that model dielectric absorption. However, in defense of the test, I do appreciate that it is not the intention to seek a broadband null, thus compensating for all parasitics, as these are reflected in the error signal. However, the central question remains, that if the circuit can be minimised at any preselected frequency, which frequency - if any - should be selected?

This latter observation is the nub of the problem and it is why it is fundamentally important to minimise the error for a non-specific test signal, otherwise the residual is just an artefact of linear distortion resulting from a particular alignment of the error test circuit and frankly, tells us very little. The best test signal is pro bably bandlimited white noise tailored to match the audible spectrum,where the optimum alignment would yield a minimum rms value of the error signal. Such a test exercises

the total range of operation of the error circuit in a way that is more representative of non specific audio signals.

I personally feel that the error test circuit should employ a more representative capacitor model, the elements of which are then optimised to reduce the error signal: the parameters of the model then gain a greater importance than the characteristics of the error and once all the linear distortions under 'normal' theory have been properly accounted, the residual error may then yield some hidden secret. Note also how important it is to have an error amplifier where the gains of the non-inverting and inverting inputs are identical ($\alpha = 0$), otherwise a false balance and a false interpretation of the error results.

Finally, I would like to emphasise that the error test as presented, though related to the notion of transfer-error function, is not identical: in the test circuit the output error is $A - A_t$, whereas the transfer-error function is $(A-A_t)/A_t$, (A → actual transfer function, A_t → target transfer function).

Hence for the example of Fig. A1, the transfer - error function E(f) is:

$$E(f) = A \left[\frac{(1 - T_1/T_0) + j\omega (\tau_1 - \tau_0 T_1/T_0)}{1 + j\omega (T_1 + \tau_1)} \right]$$

where τ_0, T_0 are the reference time constants and T_1, τ_1 the capacitor - under - test time constants.

It is important to note, however, that even if questions are raised about the nature of the error signal, the fact that an error exists when compared against a high quality reference capacitor, when (some) first - order parasitics are accounted for, is positive evidence for non-ideal capacitor performance.

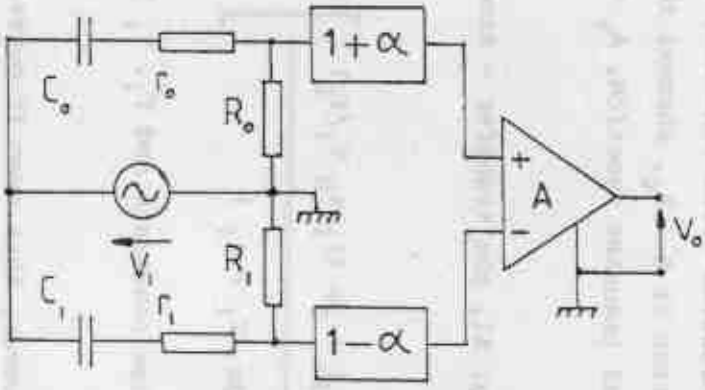

Fig. A1 Basic capacitor error test circuit after John Curl

The Essex Echo: Unification - Track 2

A transmission line is an assembly of two or more conductors that are used to guide electromagnetic energy from source to destination. The mathematics of this system are defined by the equations of Maxwell (1,2) which describe the mechanics of wave propagation in space, where some of the background was presented in the Essex Echo on interconnects (3). The essence of this model is that there exists a natural exchange of energy between the electric and magnetic fields, where the fields act as energy reservoirs that can be considered as a continuum of capacitance and inductance within the stuff of space.

The modelling of the electric and magnetic fields profess to offer a deeper understanding of the nature of space and, in a sense, this is true as we can precisely predict the outcome of most electromagnetic systems. However, we should appreciate that the equations of Maxwell are strictly only a mathematical construction, there is in fact minimal information as to the substance of natural structures. Nevertheless, the theoretical predictions of Maxwell are not in question and his results will serve as well in describing interconnect and capacitor performance. However, before commencing the study of transmission lines, I would like to make some basic comment for tutorial value as to the nature of electric and magnetic fields.

Digression: Some observations on electric and magnetic fields

An electric field $\overline{E}$ volt/metre, is a distributed stress-event in space, the effect of which is measured as the force $\Delta\overline{F}$ newton exerted on a given charge ΔQ coulomb, where,

$$\overline{E} = \frac{\Delta\overline{F}}{\Delta Q} \Bigg|_{\lim \Delta Q \to 0}$$

[the direction of $\overline{E}$ is the same as $\Delta\overline{F}$]

The electric field can in principle have two constituent components, one due to static charge interaction and the second dynamic charge (or more generally, field) interaction. The static component of the electric field finds its origin in the classic observation of the force between two point charges, attributed to the Frenchman, Charles Coulomb (1,2), a colonel in the French Army Engineers, where,

$$\bar{E}_r = \frac{Q_2}{4\pi\epsilon_r\epsilon_o}\,\frac{\bar{r}}{r^3} \quad \text{and} \quad \bar{F} = Q_1\,\bar{E}_r$$

[$\bar{E}_r$ is the electric field at a displacement $\bar{r}$ metre from charge Q_2 coulomb and $\bar{F}$ is the force exerted on a charge Q_1 at the point of observation of $\bar{E}_r$]

Embedded in the expression for $\bar{E}_r$, are two constants, the permittivity of free space ϵ_o, ($\epsilon_o = 8.855.10^{-12}$ F/m) and the relative permittivity or dielectric constant ϵ_r, ($\epsilon_r = 1$, for vacuum). These quantities relate experimental information about both the space containing the charges and of dielectric polarisation (1,2); they link charge, the 'cause' of the electric field, to $\bar{E}_r$, the observed 'effect' of the field. However, although Coulomb's equations accurately determine the forces between static charges, experimental observation reveals they do not predict the force (say between Q_1, Q_2) when there is motion between the charges. There is now an extra component of force due to their velocity. The more general expression for force is then described by the Lorentz equation (1,2),

$$\bar{E}_T = \{\,\bar{E}_r + \bar{V}_x\bar{B}\,\}, \quad \text{thus} \quad \bar{F} = Q_2\,\bar{E}_T$$

Total $\bar{E}$ field	Static field	Dynamic field

The expression shows the total electric field is the summation of the static (Coulomb) electric field $\bar{E}_r$ and a dynamic electric field $\{\bar{V}_x\bar{B}\}$, where $\bar{V}$ is the velocity of Q_1 and $\bar{B}$ the magnetic flux density.

The charge motions of Q_1, Q_2 are generally observed with respect to a reference framework. To account for the inter-charge forces within this framework, the magnetic fields $\overline{H}$ ampere-turn (magnetising force) and $\overline{B}$ tesla (magnetic flux density) are introduced. The motion of Q_2 (say) with respect to the framework in a sense dynamically stresses the surrounding space thus constituting the field $\overline{H}$. However, if the $\overline{H}$ field itself changes or an observer moves with respect to the $\overline{H}$ field, then an electric field ($\overline{E} = \Delta\overline{F}/\Delta Q_1$) is required in the model to account for the experimentally observed force on charge. Hence, the $\overline{H}$ and $\overline{B}$ fields are again 'cause' and 'effect' events. In our example, $\overline{H}$ results from the motion of Q_2 (a current) and $\overline{B}$ is measured from the force on a moving charge Q_1 travelling with velocity $\overline{V}$, i.e. $[Q_1 \overline{V}_x \overline{B}]$. A constant of space, the permeability $\mu_r\mu_o$ ($\mu_o = 4\pi.10^{-7}$ H/m, $\mu_r = 1$ for vacuum), can then be determined that links $\overline{B}$ and $\overline{H}$ by the constitutive equation $\overline{B} = \mu\overline{H}$. The component of force $[Q_1 \overline{V}_x \overline{B}]$ is that expressed in the Lorentz equation. In a more general sense Maxwell embedded these notions in the familiar equations (1,2,3),

$$\text{curl } \overline{H} = \overline{J} + \frac{\partial \overline{D}}{\partial t} \quad , \qquad \text{curl } \overline{E} = \frac{-\partial \overline{B}}{\partial t}$$

We can visualise, therefore, the concept of magnetism as being an intrinsic property of space that is necessary to account for the extra component of force experienced when charge is in motion. Observe how a magnetic field is always associated with moving charge (electric currents) or via Gauss's theorem (1,2), a changing electric flux density. Even permanent magnets and ferromagnetism are associated with charge motion, such as electron spin, at a sub-atomic level.

For example, linking our digression with the force equation $f = \{Bl\}i$ described on Track 1, we observe this result follows directly from the Lorentz equation where, effectively, Q_1 and $\overline{V}$ are combined to constitute a current i, which flows within the magnetic field $\overline{B}$, itself a function of sub-atomic charge motion within the permanent magnet. The static component of $\overline{E}$ is zero as there is no net static electric field.

Also, since a transmission line has moving charge (current) in the conductors, it follows that a complete system must model, in a distributed sense, the mutual interdependence of the electric and magnetic fields, which are described in full by the Maxwellian equation set (3). Our discussions will, therefore, attempt to demonstrate the union of electromagnetic theory and transmission line systems.

Transmission line theory

My critics will argue that interconnect performance can be described quite adequately in conventional terms, using a lumped LCR network. In part this is true for inductance and capacitance within the audio band, but it deviates for the loss field within the conductors. However, my purpose is to build a more general theory and to present to the reader the essential elements of a transmission line.

The aim of the work, therefore, presented in this essay is to model the principle features of an interconnect and large-area capacitor using transmission line theory. The theory must take account of both the dielectric properties and the structural geometry (within reason) and in particular, the internal loss fields within the guiding conductors.

The latter effect is specifically relevant to audio interconnects. Due to the high conductor conductivity (σ for cu is $5.8.10^{-7}$ S/m), the internal loss wave that propagates in a radial direction and defines the axial current distribution, has a very low velocity v within the audio band, that is typically 1 to 60 m/s for copper, where

$$v = \left\{\frac{2\omega}{\mu_o \mu_r \sigma}\right\}^{\frac{1}{2}} \quad \text{m/s}$$

As further evidence of the significance of the loss field see Stanley Kelly's contribution in HFN (4_f)

ω, angular frequency, rad/s

μ_o, permeability of free space, H/m

μ_r relative permeability ($\mu_r = 1$ for free space)

σ, conductivity, S/m

It is the low velocity of propagation that makes skin depth significant at audio frequencies and for accuracy the transmission line analysis must include its effect.

The strategy adopted in this series of articles is to estimate the transfer function of a finite length of transmission based initially upon an elemental section of the line, as this possibly represents a more familiar concept. An alternative methodology is to solve a series of differential equations describing wave motion, where readers interested in this approach are referred to communications' texts, for example by Connor (5). However, the analyses are equivalent as the elemental line is in effect a representation of the differential equations, which we choose to investigate here in the frequency domain.

We proceed by first analysing the characteristic impedance and transfer function of the elemental (very short) transmission line shown in Fig. 1, where the conductors are assumed symmetrical and the line is of length ΔL metre. The lumped circuit of the elemental line consists of two series impedances and one shunt admittance: the series impedance relate to the internal conductor fields and external magnetic field, while the shunt admittance relates to the external electric field. Hence, the lumped elements represent the local, orthogonal magnetic and electric fields of the transmission line, respectively.

There is a voltage ΔV across the series impedances of the line, when a signal is applied, which is due to two factors:

(i) the inductance, i.e. there is a changing magnetic field flowing between the conductors that generates, by Faraday, a voltage $L_e \frac{di}{dt} \Delta L$, where inductance L_e is a function of line geometry and dielectric

(ii) the loss field within the conductors which exhibit in general both a frequency dependent resistance and reactance

Superimposing the factors (i) and (ii), the total impedance/metre of the series elements can be expressed as (a + jb) ohm/m, (j is the complex algebra operator $\sqrt{-1}$).

The shunt element that models both the characteristics of the dielectric and the line geometry is similarly represented, though we choose to use the admittance/metre notaton (c + jd) S/m. In a general form, the shunt element can include both resistive and capacitive components to model dielectric loss and dielectric absorption.

Consequently, the parameter set {a, b, c, d} where each element is itself a function of frequency, describe the principle elements of a transmission line, which relate directly to the static material and geometry of the system. This latter observation significantly simplifies the analysis, where on Track 3 we shall discuss the procedures and show how the parameter set can include both skin depth and dielectric absorption.

It is important to note that a complete transmission line is formed by a cascade of elemental sections of the form shown in Fig.1. However, when the limit $\Delta L \to 0$ is taken, the analysis becomes applicable to the distributed system and there is no loss of generality, as occurs, for example, with lumped-element approximations.

Characteristic Impedance

The characteristic impedance Z_0 is the input impedance of a transmission line of infinite length, or more reasonably the input impedance of a finite length of line that itself is terminated in its characteristic impedance, which implies zero energy reflection at the termination. This latter observation allows Z_0 to be extracted from the elemental transmission line shown in Fig.2 in the limit as $\Delta L \to 0$.

Since the input and load impedances are equal,

$$Z_0 = \overbrace{(a + jb)\,\Delta L}^{\text{series element}} + \overbrace{\frac{Z_0}{(1 + Z_0(c + jd)\Delta L)}}^{\text{shunt element}//Z_0}$$

Neglecting terms in ΔL^2 as $\Delta L \to 0$ and rearranging,

$$Z_0 = \left[\frac{a + jb}{c + jd}\right]^{\frac{1}{2}}$$

To aid evaluation of the modulus and phase of Z_o, let,

$$Z_o = R_0 \, e^{j\phi_0}$$

where,

$$R_0 = \left[\frac{a^2 + b^2}{c^2 + d^2}\right]^{\frac{1}{4}}$$

$$\phi_o = 0.5 \left\{\arctan\left(\frac{b}{a}\right) - \arctan\left(\frac{d}{c}\right)\right\}$$

[For Z_o to be real, ad = bc implying a suitably lossy dielectric is desirable!]

The evaluation of Z_o as well as representing an informative parameter in its own right, is also a necessary intermediate stage in specifying the transmission line model, which will be shown to reduce simply to a knowledge of Z_o and the propagation constant γ (5).

Transfer function of matched transmission line of finite length

The next stage is to develop the voltage-transfer function over a finite line of length L metre when the line is terminated in its characteristic impedance, Z_o. This procedure is an evolutionary step in developing the general case with an arbitrary load impedance. It is important to note that a transmission line terminated in its characteristic impedance does not reflect electromagnetic energy at the termination.

Consider the voltage-transfer function $A(\Delta L)$ of the elemental line shown in Fig.2. The calculation is straightforward and is an extension of the potential divider rule, where again ignoring terms in ΔL^2 as the limit $\Delta L \to 0$ is taken,

$$A(\Delta L) = \frac{1}{1 + \left(\frac{a + jb}{Z_o}\right)\Delta L}$$

However, substituting the earlier result for Z_o and defining the parameter γ as,

$$\gamma = [(a + jb)(c + jd)]^{\frac{1}{2}}$$

the transfer function reduces to

$$A(\Delta L) = \left[\frac{1}{1 + \gamma \Delta L}\right]$$

To extend the result to a line of finite length L metre, consider a cascade of N elementary networks, where

$\Delta L = \frac{L}{N}$] i.e. line of length L is composed of N sections, each of length ΔL

whereby the transfer function of the finite line A(L) is,

$$A(L) = \left[\frac{1}{1 + \gamma \frac{L}{N}}\right]^{N} \qquad \lim \begin{cases} \Delta L \to 0 \\ N \to \infty \end{cases}$$

Using the binomial series expansion (see Appendix 4) and noting that for large N, $N \approx N - 1 \approx N - 2$ etc, then

$$A(L) = 1 - \left(\frac{\gamma L}{L}\right)_1 + \left(\frac{\gamma L}{L}\right)^2_2 - \ldots$$

i.e. this is the exponential series expansion of $e^{-\gamma L}$, (again see Appendix 4), whereby, $A(L) = e^{-\gamma L}$

This result is compatible with the expression for a propagating electromagnetic wave derived in the earlier Essex Echo (3), where the wave envelope decays as an exponential function of distance. The expression for A(L) enables the amplitude and phase responses for a correctly matched line to be calculated, though rearrangement is necessary to extract the result; this method is shown in Appendix 1.

Transfer function of unmatched line of finite length

The final analysis stage is to generalise the model to account for arbitrary terminating impedance. The complication arises because at an impedance mismatch a component of electromagnetic energy undergoes reflection which clearly modifies the transfer function. In principle,

reflection occurs at both ends of the transmission line; we therefore have an infinite series of reflections that can be likened to the effect where two mirrors are faced opposite to each other and the replicated image is observed to extend way into the distance. In fact, this phenomena is precisely the same effect though the wave propagation is in free spaces and the mirrors are short circuit terminating impedances (notice how distortion of the mirror surfaces that form the reflecting impedance, limit the resolution of the distant images as they merge into a fuzzy continuum).

In Fig.3, a simplified representation of an interconnect is shown together with a two-port impedance matrix equation and describes the relationship between voltage and current - note, in particular, the definition of voltage and current direction, which facilitates input/output symmetry:

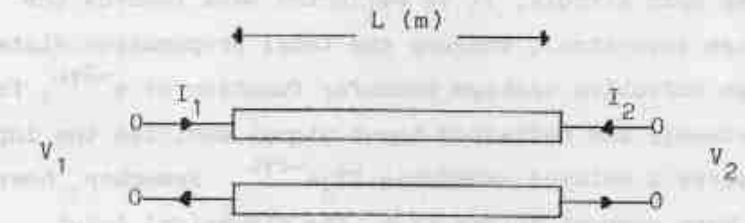

$$\begin{bmatrix} V_1 \\ V_2 \end{bmatrix} = \begin{bmatrix} Z_{11}(L) & Z_{12}(12) \\ Z_{21}(L) & Z_{22}(L) \end{bmatrix} \begin{bmatrix} I_1 \\ I_2 \end{bmatrix}$$

Fig. 3 Impedance matrix of symmetrical transmission line

The [Z] matrix equation is a short-hand notation for (in this case) two simultaneous equations where the [Z] elements define the parameters of the transmission line and we seek to equate [Z] to $[Z_0, \gamma]$.

However, as the line is both symmetrical and a passive network, the four elements in [Z] reduce to two since, $Z_{11}(L) = Z_{22}(L)$ and $Z_{12}(L) = Z_{21}(L)$. Hence, to complete the model only the impedances $Z_{11}(L)$, $Z_{12}(L)$ are required.

(i) $Z_{11}(L)$, input impedance of transmission line when output is open circuit

An open-circuit output ($I_2 = 0$) implies that there is a total signal reflection at the impedance discontinuity; also $I_2 = 0$ reduces the matrix equation to,

$$V_1 = Z_{11}(L)\, I_1, \quad \text{and} \quad V_2 = Z_{21}(L)\, I_2$$

which enables

$$Z_{11}(L) = V_1/I_1$$

to be calculated, i.e. $Z_{11}(L)$ is the input impedance of the transmission line when the output is open circuit.

Imagine that I_1 is sinusoidal: if the line were of infinite extent then the input impedance is simply Z_0 as $V_1 = I_1 Z_0$. However, when the signal arrives at the open circuit, it is reflected back towards the input (without voltage inversion), whereby the total propagation distance becomes 2L, giving an effective voltage transfer function of $e^{-2\gamma L}$, for the first pass. Obviously the reflected input signal modifies the input impedance and we observe a delayed impedance $2Z_0 e^{-2\gamma L}$. Remember, however, that as the line is here current driven (i.e. the sinusoidal input current is specified), the driving source impedance is also infinite, and the first-pass reflected signal is once again passed back into the interior of the line (again without voltage inversion), whereby the process is repeated until eventually the multi-reflected signal decays to insignificance.

The total input voltage which is a summation of all the reflections is therefore expressed as an infinite series,

$$V_1 = I_1 Z_0 \left[1 + 2e^{-2\gamma L} + 2e^{-4\gamma L} + \ldots\right]$$

Rearranging and noting the expression contains a geometric series (see Appendix 4), the input impedance $Z_{11}(L) = V_1/I_1$ is,

$$Z_{11}(L) = Z_0\left[\frac{1 + e^{-2\gamma L}}{1 - e^{-2\gamma L}}\right]$$

This expression is a complete description of $Z_{11}(L)$. However, extracting $e^{-\gamma L}$ from numerator and denominator together with a quick reminder of the hyperbolic functions (see Appendix 2), reveals a short-hand notation, where

$$Z_{11}(L) = Z_0\left[\frac{e^{\gamma L} + e^{-\gamma L}}{e^{\gamma L} - e^{-\gamma L}}\right] = Z_0\left[\frac{\cosh(\gamma L)}{\sinh(\gamma L)}\right]$$

i.e. $Z_{11}(L) = Z_0 \coth(\gamma L)$

The development of this result may have appeared somewhat tortuous, but observe how the logic encapsulates the concepts of characteristic impedance, transfer function and reflection at an impedance mismatch, where for an open-circuit termination, the voltage is reflected with the same polarity (it is inverted for a short circuit).

(ii) $Z_{21}(L)$, output-input transimpedance, output open circuit

The second and final unknown matrix element is the term $Z_{21}(L)$, where we recall that when $I_2 = 0$ (output open circuit), $V_2 = Z_{21}(L)\, I_1$. Since in (i) the ratio V_1/I_1 was determined, we need only analyse the voltage transfer function V_2/V_1 of a line of L metre with open-circuit output; it then follows that,

$$Z_{21}(L) = \left[\frac{V_1}{I_1} \cdot \frac{V_2}{V_1}\right]_{I_2 = 0} = \left[Z_{11}(L) \cdot \frac{V_2}{V_1}\right]_{I_2 = 0}$$

The key to determining V_2/V_1 is to extend the earlier result for the transfer function of a finite, matched line by again observing reflection at each end (note-sign in series, sending end is voltage driven hence effectively short circuit), whereby

$$\left.\frac{V_2}{V_1}\right|_{I_2 = 0} = 2\left[\underbrace{e^{-\gamma L}}_{\text{1st pass...}} - \underbrace{e^{-3\gamma L}}_{\text{2nd pass...}} + \underbrace{e^{-5\gamma L}}_{\text{3rd pass ... etc ...}} - \ldots\right]$$

Again extracting $e^{-\gamma L}$ and noting the geometric series,

$$\left.\frac{V_2}{V_1}\right|_{I_2 = 0} = \left[\frac{2\,e^{-\gamma L}}{1 + e^{-2\gamma L}}\right] = \left[\frac{2}{e^{\gamma L} + e^{-\gamma L}}\right]$$

Hence, using the result from (i) for $Z_{11}(L)$,

$$Z_{21}(L) = \left[\frac{2\,Z_0}{e^{\gamma L} - e^{-\gamma L}}\right]$$

where applying the hyperbolic functions listed in Appendix 2,

$$Z_{21}(L) = Z_0\,\mathrm{csch}\,(\gamma L)$$

The [Z] matrix parameters expressed in terms of the characteristic impedance Z_0 and propagation constant γ are now complete, where the transmission line model is expressed,

$$\begin{bmatrix} V_1 \\ V_2 \end{bmatrix} = Z_0 \begin{bmatrix} \coth(\gamma L) & \mathrm{csch}(\gamma L) \\ \mathrm{csch}(\gamma L) & \coth(\gamma L) \end{bmatrix} \begin{bmatrix} I_1 \\ I_2 \end{bmatrix}$$

where, $Z_0 = \left[\frac{a + jb}{c + jd}\right]^{\frac{1}{2}}$

$$\gamma = [(a + jb)\,(c + jd)]^{\frac{1}{2}}$$

Conclusion

As earlier discussed, the parameter set {a, b, c, d} are directly related to the static characteristics of the line, that include inductance, capacitance and the internal conductor loss mechanism. The advantage of our approach is that the matrix equation models exactly a distributed system and does not require the complexity of multi-node analysis of a finite, lumped-element model of the type illustrated in Fig.4, which at best is only approximate for wide-band analysis.

The distributed model readily accommodates any load impedance providing it is numerically determinate over the band of frequency required. Effectively, specifying the load impedance locks together V_2 and I_2 in the impedance matrix, where $Z_L = -V_2/I_2$, (the - sign appears as the matrix was defined with output current flowing into the network). Consequently, the model is applicable to either loudspeaker-interconnect systems or large area capacitors (the latter by putting $Z_L = \infty$). We will show on Track 3 how skin depth phenomena can be incorporated without loss of generality, where the mechanism is itself an open-circuit transmission line.

This second track has been fairly rigorous in its presentation, but I hope the detail will have given at least some insight into the theory of transmission lines. I personally believe it is important to grasp the underlying principles of distributed wave propagation; they are the key to a more complete understanding of audio error mechanisms. Of such stuff errors are propagated ...

To be continued...

References

1. Hayt, W.H., Jr., Engineering Electromagnetics, 3rd edition, McGraw-Hill Inc., ISBN 0-07-027390-1, 1974

2 Wangsness, R.K. Electromagnetic Fields, John Wiley and Sons, Inc., ISBN 0-471-04103-3, 1979

3 Hawksford, M.J. "The Essex Echo: Maxwellian theory and interconnect memories", HFN and RR, Vol.30, No.8, pp.27-33, August 1985

4 Kelly, S. "... about conductor science", Letter to the Editor, HFN and RR, Vol.30, No.10, p.17, October 1985

5 Connor, F.R. Wave Transmission, Edward Arnold (Publishers) Ltd., ISBN 0-7131-3278-7, 1972

APPENDIX 1

Observations on evaluating γ

The propagation constant as expressed in this article is not in a form that allows direct evaluation. In this Appendix, the mathematics for extracting the attenuation and phase constants α and β are presented.

As in (3), γ can be written as

$$\gamma = \alpha + j\beta$$

i.e. $$\alpha + j\beta = \{(a + jb)(c + jd)\}^{\frac{1}{2}}$$

hence,

$$m = (\alpha^2 + \beta^2)^{\frac{1}{2}} = \{(a^2 + b^2)(c^2 + d^2)\}^{\frac{1}{4}}$$

$$n = \frac{\beta}{\alpha} = \tan\left[0.5\left[\arctan\left(\frac{b}{a}\right) + \arctan\left(\frac{d}{c}\right)\right]\right]$$

whereby, putting $\beta = n\alpha$,

$$\alpha = \frac{m}{\sqrt{1 + n^2}} \quad , \quad \beta = \frac{m\,n}{\sqrt{1 + n^2}}$$

If we have a sinusoidal wave propagating in a matched cable, then following (3), we can write

$$v(z) = V e^{-\alpha z} \sin(\omega t - \beta z)$$

whereby the real part of γ determines the attenuation and the imaginary part, the phase at a distance z along the cable.

APPENDIX 2

Hyperbolic functions

To facilitate a greater appreciation of the mathematics used in this series of articles, the following definitions and relationships of the hyperbolic family of functions are presented:

$$\sinh(x) = \frac{e^{x} - e^{-x}}{2} \qquad \cosh(x) = \frac{e^{x} + e^{-x}}{2}$$

$$\operatorname{csch}(x) = \frac{1}{\sinh(x)} \qquad \operatorname{sech}(x) = \frac{1}{\cosh(x)}$$

$$\tanh(x) = \frac{\sinh(x)}{\cosh(x)} \qquad \coth(x) = \frac{\cosh(x)}{\sinh(x)}$$

$$\cosh^{2}(x) - \sinh^{2}(x) = 1 \qquad 1 - \tanh^{2}(x) = \operatorname{sech}^{2}(x)$$

$$\coth^{2}(x) - 1 = \operatorname{csch}^{2}(x)$$

If x is complex, where $x = (\alpha + j\beta)z$, then

$$e^{(\alpha + j\beta)z} = e^{\alpha z}\, e^{j\beta z} = e^{\alpha z}(\cos \beta z + j \sin \beta z)$$

$$e^{-(\alpha + j\beta)z} = e^{-\alpha z}\, e^{-j\beta z} = e^{-\alpha z}(\cos \beta z - j \sin \beta z)$$

APPENDIX 3

Special case of lossless transmission line

For the special case where a transmission line has negligible conductor resistance, which is not normally applicable to audio interconnects, then the attentuation constant $\alpha \rightarrow 0$. When $\alpha = 0$, the propagation constant $\gamma = j\beta$, whereby the impedance matrix equation involves only trigonometric functions and is written

$$\begin{bmatrix} V_1 \\ V_2 \end{bmatrix} = -jZ_o \begin{bmatrix} \cot(\beta L) & \csc(\beta L) \\ \csc(\beta L) & \cot(\beta L) \end{bmatrix} \begin{bmatrix} I_1 \\ I_2 \end{bmatrix}$$

where, $\cot(\beta L) = \dfrac{\cos(\beta L)}{\sin(\beta L)}$, $\csc(\beta L) = \dfrac{1}{\sin(\beta L)}$

APPENDIX 4

Binomial and geometric series

The three series expansions used in the articles are listed here.

Binomial [$|x| < 1$]

$$(1 + x)^N = 1 + Nx + \frac{N(N-1)}{L^2} x^2 + \ldots + \frac{L^N}{L(N-r)\,L^r} x^r + \ldots$$

Geometric [$x \neq 1$]

$$1 + x + x^2 + \ldots + x^{N-1} = \frac{1 - x^N}{1 - x}$$

Exponential

$$1 + x + \frac{x^2}{L^2} + \frac{x^3}{L^3} + \ldots + \frac{x^r}{L^r} + \ldots = e^x$$

N.B. L is factorial sign, where for example $L^3 = 3.2.1 = 6$

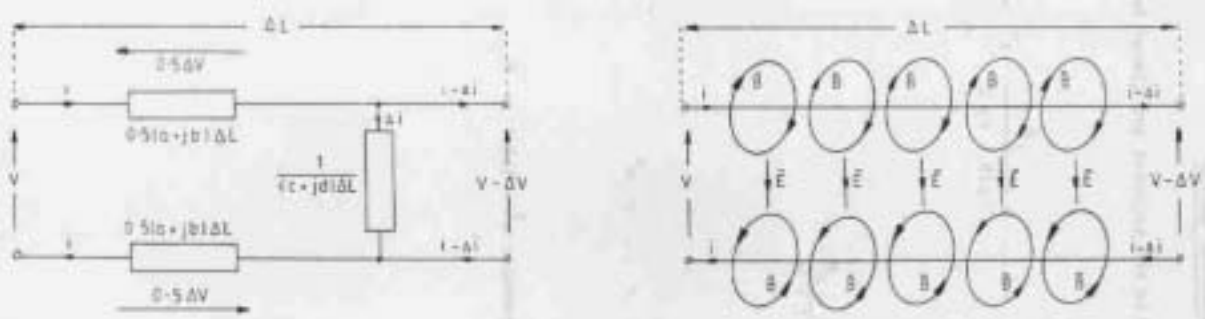

Fig.1 Elemental and symmetrical transmission line

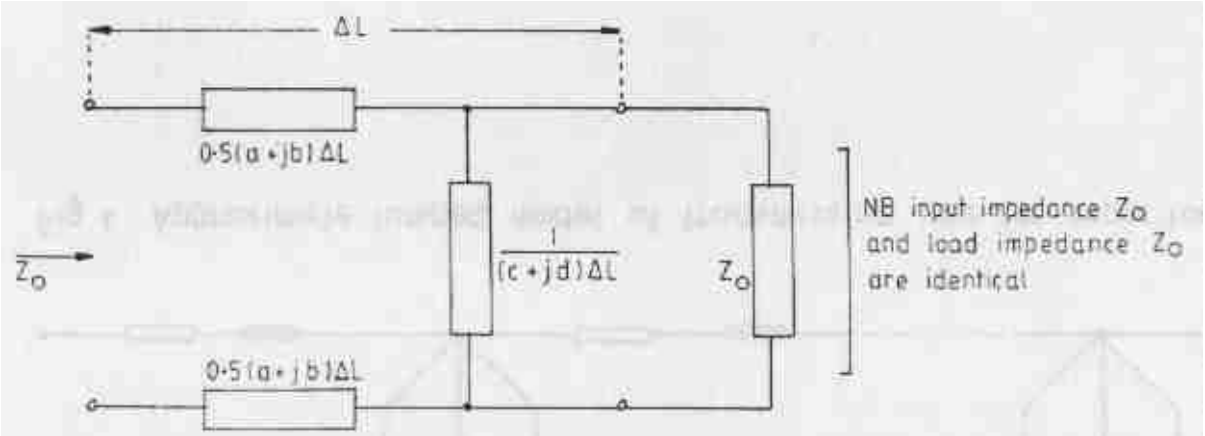

Fig. 2 Computational model for characteristic impedance of elemental line of length ΔL metre

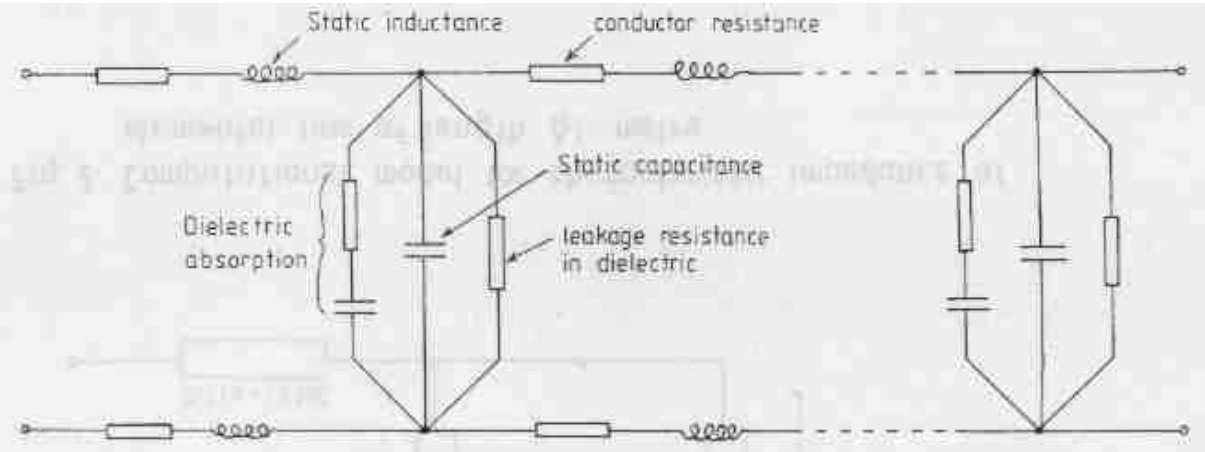

Fig. 4 Approximate lumped model of transmission line (or capacitor)

THE ESSEX ECHO: UNIFICATION - TRACK 3

The basic analysis for a linear interconnect of both arbitrary length and load termination was completed on Track 2 in the current series of essays (1), where in principle the transfer characteristics and input impedance are now calculable, providing there exists determinate data on the load impedance. However, the model is not yet accessible, as we need to relate the transmission line parameter set {a, b, c, d} (1) to the static characteristics of actual interconnects and to include the effect of internal conductor loss fields (2). The aims of this third essay are to examine the static parameters using electromagnetic theory and to extract the model elements to account for skin depth phenomena using transmission line theory.

Our study continues by calculating the static capacitance and inductance of two classic interconnect constructions using electromagnetic theory, where I am confident that many readers will welcome the opportunity for revision of their earlier electromagnetic courses (inluding all ex-electronics Essex graduates, and to those reading HFN in Hong Kong, Singapore and Malaysia - a special 'Hi'!). The two constructions are illustrated in Figs. 1a, b: the coaxial system is composed of two concentric cylinders of inner and outer radii r_1 and r_2 (metre) where $r_2 > r_1$, while the symmetrical (thin conductor $r \ll R$) parallel transmission line has two conductors each of radii r (metre) separated between centres by R (metre).

The question of skin depth does not arise in the static analysis. It is a dynamic property which will be discussed later in this article. For conciseness, we will investigate the coaxial construction in greater detail and state only the results for the parallel conductor systems; though be assured that the same analysis procedures apply in each case.

Mutual, static capacitance of coaxial interconnect

The static capacitance per unit length of a coaxial transmission line, C_c F/m, is defined,

$$C_c = Q/V \quad F/m$$

where charges of Q and -Q (coulomb/metre) reside respectively on the two conductors and establish a potential difference V volt between the conductors. Providing the geometry is rigid and the dielectric linear, then C_c is a constant that is related directly to the interconnect structure and dielectric permittivity $\epsilon_r \epsilon_o$ F/m.

To determine the capacitance, the potential difference is calculated for a given charge and geometry. This is achieved by first evaluating the electric field E_r V/m at a radius $r(r_2>r>r_1)$ in the space between the coaxial conductors, whereby V follows as,

$$V = \int_{r_1}^{r_2} \bar{E}_r . d\bar{r}$$

The cylindrical symmetry of the coaxial structure implies that the electric field $\bar{E}_r$ is directed everywhere radially and has a constant magnitude for a constant radius. We estimate $\bar{E}_r$ for a given charge as follows.

From the theorem of Gauss (3), any closed surface that contains a total charge Q, will experience a net electric flux of $\epsilon_r \epsilon_o \bar{E}$ through the surface that is numerically equal to the charge, irrespective of distribution or surface geometry. This is expressed in general as,

$$\iint_S \epsilon_r \epsilon_o \bar{E} . d\bar{S} = Q$$

and is directly related to the Maxwellian equation, $\mathrm{div}(\epsilon_r \epsilon_o \bar{E}) = \rho$, (3).

To calculate $\bar{E}_r$ (at a radius r), imagine the closed Gaussian surface S to be a cylinder of radius r and length 1 metre, centred about the inner conductor of a representatively long (theoretically infinite) length of interconnect. Also, because of the radial field pattern, there is no flux of $\epsilon_r \epsilon_o E_r$ through the end caps of the cylindrical surface: the required surface area is simply the curved surface, $2\pi r$ area/metre, i.e.

$$E_r = \frac{Q}{2\pi \epsilon_r \epsilon_o r} \text{ volt/metre}$$

(Note: E_r implies the modulus of vector $\bar{E}_r$)

where the potential difference between the conductors r_1, r_2 follows from

the integral of E_r as,

$$V = \int_{r_1}^{r_2} \frac{Q}{2\pi \varepsilon_r \varepsilon_o} \frac{dr}{r} = \frac{Q}{2\pi \varepsilon_r \varepsilon_o} \ln\left[\frac{r_2}{r_1}\right] \text{volt}$$

[Note that for a static field the integral of $\overline{E}$ depends only on the end points of integration, the field is conservative since curl $\overline{E}$ = 0]

Hence, the static capacitance per metre C_c is

$$C_c = \frac{2\pi \varepsilon_r \varepsilon_o}{\ln\left[\frac{r_2}{r_1}\right]} \quad \text{farad/metre}$$

The expression for C_c demonstrates that the capacitance is principally a function of the ratio of the conductor radii and not their absolute dimension. The linear dependance upon the relative and absolute permittivities ε_r, ε_o should also be noted as this in principle affects the selection of the shunt transmission line parameters, (c + jd) siemen/metre.

Mutual static inductance of coaxial interconnect

A short circuit length of coaxial transmission line carrying a constant current I ampere, exhibits a magnetic field that form by symmetry a circular path around the inner conductor and occupies only the space between the conductors. Evaluating the total magnetic flux per metre (ϕ weber/metre) then allows the loop inductance L_c henry/metre to be expressed as

$$L_c = \frac{\phi}{I} \quad \text{henry/metre}$$

[compare the duality with the capacitance, $C_c = Q/V$]

To calculate ϕ, we first estimate the magnetic flux density B_r tesla at a radius r ($r_1 < r < r_2$) using Ampere's circuital law (3),

$$I = \int_{C_r} \frac{\overline{B}_r}{\mu_r \mu_o} \cdot d\overline{l} = \frac{B_r}{\mu_r \mu_o} 2\pi r, \text{ i.e. } B_r = \frac{\mu_r \mu_o I}{2\pi r}$$

this equation follows directly from the Maxwellian equation (2.3) set where,

$$\text{curl}\ (\bar{B}/\mu_r \mu_o) = \bar{J} + \frac{\partial}{\partial t}(\varepsilon_r \varepsilon_o \bar{E})$$

The integration is simplified by symmetry, as B_r and has a constant magnitude at a radius r allowing the integration contour C_r to be a circular path of circumference $2\pi r$. The Amperian integral also reveals that for $r>r_2$, the flux is zero as there is no net current flow through the surface generated by C_r, hence all the magnetic flux is concentrated in the space between the conductors.

The total flux ϕ is most simply estimated by evaluating the total flux of $\bar{B}_r$ taken over the rectangular surface ABCD, shown in Fig. 1(a). The surface is positioned with AB, CD radial and BC, DA set to 1 metre, orientated axially to just touch the two conductors. The total flux/metre must then all pass through ABCD and is evaluated as,

$$\phi = \iint_{\text{surface ABCD}} \bar{B}_r . d\bar{s} = \int_{r_1}^{r_2} \frac{I \mu_r \mu_o}{2\pi} \frac{dr}{r} = \frac{I \mu_r \mu_o}{2\pi} \ln\left[\frac{r_2}{r_1}\right]$$

whereby the loop inductance/metre follows from $L_c = \phi/I$

$$L_c = \frac{\mu_r \mu_o}{2\pi} \ln\left[\frac{r_2}{r_1}\right] \quad \text{henry/metre}$$

The results for C_c and L_c show that the geometry of the conductors together with $\varepsilon_r \varepsilon_o$ and $\mu_r \mu_o$ allow a precise prediction of the capacitance and inductance per metre of interconnect. Similarly, an investigation of the parallel conductor transmission line reveals for $r<<R$,

$$L_p = \frac{\mu_o \mu_r}{\pi} \ln\left[\frac{R}{r} - 1\right], \quad C_p = \frac{\pi \varepsilon_o \varepsilon_r}{\ln\left[\frac{R}{r} - 1\right]}$$

It is informative to observe how the boundary behaviour of the conductors gives an image of the electromagnetic activity within the space linking the conductors.

Product of capacitance and inductance

The expressions derived for the two interconnect geometries demonstrate an interesting property when the product of capacitance/metre and inductance/metre is taken, namely that the product in each case equals $\{\varepsilon_r \varepsilon_o \mu_r \mu_o\}$.

This observation shows there to be fundamental linkage between L and C that is impossible to separate for the given examples. Hence, when the capacitance increases, the inductance must fall and vice-versa. The central question is: Do these specific relationships apply to all interconect constructions irrespective of geometry? My answer is a qualified 'Yes'. There appears to be little problem when the conductors are straight and parallel. However, allow the conductors to spiral or to be coiled in some geometric more adventurous way and we then observe inter-coil coupling both capacitively and inductively. The linked flux, in a sense, define feedforward paths and we appear to enter a whole new ball game. I think this complication will be carried forward to another date as part of the problem is estimating the effective conductor length.

(c + jd) → Dielectric absorption and loss

A practical dielectric will, in general, exhibit vestiges of phenomena called dielectric absorption. In principle, dielectrics are insulators having ideally no conduction electrons free to migrate across the structure. However, when the dielectric is polarised and the bonded-electron, field patterns, aligned, charge migration does occur. Consequently, when the field is removed, there remains a degree of polarisation where it takes time for the dielectric to neutralise. This phenomena is readily demonstrable with large electrolytics: if such a capacitor is rapidly discharged and then left open circuit, the terminal potential difference slowly rises. In Fig. 2, a lumped (static) model of the shunt impedance of an interconnect/capacitor is shown, where C_1 and C_2 are capacitances/metre which, together with R_2 ohm/metre, model the dielectric absorption, i.e. try to picture the circuit operating as if it were the large capacitor example just described. Resistor R_1 ohm/metre represents the leakage resistance though, in practice, it is extremely large.

The components shown in Fig. 2 relate directly to the shunt admittance (c + jd) S/m of the transmission line model ( ), where if ω is the angular frequency rad/s, the parameters c and d can be equated to the components R_1, R_2, C_1, C_2 as

$$c = \frac{1}{R_1} + \frac{(\omega R_2 C_2)^2}{R_2 (1 + (\omega R_2 C_2)^2)}$$

$$d = \frac{\omega C_2}{1 + (\omega R_2 C_2)^2} + \omega C_1$$

For the special case of an ideal dielectric these expressions simplify to c = 0, d = ωC_e, where the (external) capacitance C_e F/m relate, for example, to the coaxial and parallel interconnects analysed earlier.

Internal conductor fields - skin depth

Skin depth has been described ( ) as resulting from an electromagnetic wave that propagates in a radial direction, within the conductors. The wave has its electric field component aligned along the conductor axis, which in turn determines the current distribution over the conductor cross-sectional area ($\bar{J} = \sigma \bar{E}$).

Because we are dealing with a propagation phenomena, the transmission line model can be used to evaluate the component of conductor impedance due to the internal fields. Since the conductor radii (non-litz) range at most to a few milli-metre, the internal wave will undergo reflection at the conductor boundary due to the gross impedance mismatch. Now I must own up that I found this area of the analysis more difficult and, at best, the results are approximate, due in principle to the geometry: consequently, when you write your letters of complaint, please address them directly to John Atkinson! (So that's why John decided to leave HFN!)

The conductor geometry is shown in Fig. 3 and is somewhat artificial.

At boundary A, let the current density be J_o, where the loss wave propagates in the z direction; noting that the current is aligned with ΔL, the elemental length of conductor. As the wave propagates from boundary A towards boundary B, it undergoes rapid attenuation as the conductor has high conductivity. At the boundary B, there is total reflection due to the impedance mismatch (conductor-dielectric); similarly the returned, further attenuated, wave is again reflected at A, and so on. It is the two mirror problem, though here the propagation velocity is very low and the attenuation high (1,2). Consequently, in estimating the current density J(z) at a depth z, the multiple reflections must be accounted (even though they rapidly decay with distance).

Considering the multiple-boundary reflections and noting the attenuation and phase over a length x is $e^{-\gamma x}$, then

initial wave ... first reflection ... 2nd reflection etc

$$J(z) = J_o \left[e^{-\gamma z} + e^{-\gamma(2L-z)} + e^{-\gamma(2L+z)} + e^{-\gamma(4L-z)} + e^{-\gamma(4L+z)} + \ldots \right]$$

where observing the power series and simplifying,

$$J(z) = J_o \left[\frac{e^{-\gamma z} + e^{-\gamma(2L-z)}}{1 - e^{-\gamma 2L}} \right]$$

The total current I is calculated by intergating J(z) over the conductor cross section,

$$I = W \int_0^Z J(z)dz = \frac{W J_o}{\gamma}$$

It has already been shown for a good conductor,(2),

$$\alpha = \beta = 1/\delta \text{ and}$$

$$\gamma = \alpha + j\beta = (1 + j)/\delta$$

where δ is the skin depth. Hence substituting for γ,

$$J_o = I(1 + j)/(W\delta)$$

The voltage ΔV appearing across an axial length of conductor ΔL is calculated from the surface electric field E; however, noting $J = \sigma E$ ($\sigma \rightarrow$ conductivity), then

$$\Delta V = E\,\Delta L = J(z = 0)\,\Delta L/\sigma$$

Hence from the expression for J(z) where z = 0 and substituting for J_o, the conductor impedance/metre due to the internal field Z_{int} (Z) is

$$Z_{int}(Z) = \frac{\Delta V}{I\Delta L} = \frac{(1 + j)}{W\,\delta\,\sigma}\left[\frac{1 + e^{-2\gamma Z}}{1 - e^{-2\gamma Z}}\right]$$

A final examination of the hyperbolic family of functions (see Track 2, Appendix 2) allows a more concise expression for the conductor internal impedance/m,

$$Z_{int}(Z) = \frac{(1 + j)}{W\,\delta\,\sigma}\ \coth(\gamma Z)$$

Although possibly contrived, the final result demonstrates a reasonable approximation to the internal field problem, assuming a non-granular conductivity. Also, the similarity with the input impedance of an open-circuit transmission line (Track 2 (1)) should be observed, where the matrix equation revealed for $I_2 = 0$, that $Z_{in} = Z_o \coth(\gamma Z)$ (in this case $L \rightarrow Z$), hence the characteristic impedance for a wave within a good conductor is $Z_o = (1 + j)/(W\,\delta\,\sigma)$.

As a final step in this tortuous treatise let us transform the expression for $Z_{int}(Z)$ into a more amenable form, you will, I trust recall that for a good conductor (2):

$$\gamma = \left[\frac{\mu\,\omega\,\sigma}{2}\right]^{\frac{1}{2}}(1 + j) = (1 + j)/\delta$$

Therefore when $\omega \rightarrow o$, $\gamma \rightarrow o$, hence

$$Z_{int}(Z)\Big|_{\omega \to 0} \simeq \frac{(1+j)}{W\,\delta\,\sigma}\left[\frac{1+\gamma Z+1-\gamma Z}{1+\gamma Z-1+\gamma Z}\right]$$

(approximation to coth (γZ) at lf)

$$\simeq \frac{(1+j)}{W\,\delta\,\sigma}\cdot\frac{1}{\gamma Z} \simeq \frac{1}{W\,Z\,\sigma} = R_{int}$$

i.e. R_{int} is the dc resistance/metre, a result that is determinable simply from a knowledge of cross-sectional area (WZ) and conductivity σ S/m, so all is well (at least at dc!).

Hence a more general expression for $Z_{int}(Z)$ is obtained by writing the expression only in terms of R_{int}, Z and δ, i.e.

$$Z_{int}(Z) = R_{int}\left[\frac{Z}{\delta}(1+j)\coth\left[\frac{Z}{\delta}(1+j)\right]\right] \text{ ohm/m}$$

This final expression is computationally quite powerful as it allows an independent selection of conductor dc resistance and conductor radius, assuming the skin depth δ is known (note δ a function of ω, μ, σ). This is useful, as a specific conductor may be assembled from a number of parallel and resistively insulated conductors, such as litz. However, there is a note of caution: clearly, there is a limit on the maximum effective radius for a given dc resistance/metre and conductivity, where for a cylindrical conductor of radius Z ,

$$Z \leq \{\pi\,\sigma\,R_{int}\}^{-0.5}$$

Estimation of series elements (a + jb)

The final calculation of the transmission line parameters a, b can now be made, thus completing the parameter set [a, b, c, d] necessary to drive the transmission line matrix equation. The series elements a, b are composed of two impedance contributions:

(i) the external magnetic field represented by, L_e H/m (this is the loop inductance) which results in an impedance $j\omega L_e$ ohm/m

(ii) the internal magnetic field represented by $Z_{int}(Z)$ ohm/m.

Consequently, the parameters a, b are calculated,

$$a + jb = j\omega L_e + 2 R_{int}\left[\frac{Z}{\delta}(1 + j)\coth\left[\frac{Z}{\delta}(1 + j)\right]\right]$$

assuming identical conductors. By equating real and imaginary parts individual functions for a and b can be extracted.

Conclusion

This track of the series has necessarily been rather rigorous in order to help establish a broader foundation to the understanding of transmission lines together with their relationship to electromagnetic theory. It has also demonstrated how the parameter set {a, b, c, d} can be calculated and equated to the interconnect properties to allow the transmission-line matrix equations to be driven. The approach has been deliberately general, so that a wide class system can be modelled that includes the audio interconnect and the large-area capacitor.

In the concluding essay, we will apply these results to a range of specific examples and give further consideration to both the field of application and the theory of the transfer-error function, particularly when linked with wave propagation.

I believe that the integration of electromagnetic theory and transmission line theory in audio systems has an important role to play in the fundamental understanding of signal propagation and equipment interfacing. In particular, the linkage between inductance and capacitance should be noted as this relates directly to the design of interconnect and capacitor systems. It is also interesting to observe how the parameters of inductance and capacitance form an image of the space between the conductors as observed at the boundary. It is analogous to the loudspeaker drive unit discussed on track 1 (4), where the electrical input impedance was shown to be an image of the unit's mechanical and acoustical domains.

The more I research the subject of audio, the greater is my appreciation that the interdependency of acoustical, mechanical and electrical

domains exhibit a fundamental union with wave propagation and transmission-line systems, projected onto a multi-dimensional spatial construct. The area is rich for a more detailed and revealing analysis, that ultimately could model all processes from microphone dust cap to brain fluidity and perceptual models. Of such stuff will expert systems be programmed ...

To be continued...

References

1 Hawksford, M.J. (Give reference to Track 2 of 'Unification' when known)

2 Hawksford, M.J. "The Essex Echo: Maxwellian theory and interconnect memories", HFN and RR, Vol.30, No.8, pp.27-33, August 1985

3 Hayt, W.H., Jr. Engineering Electromagnetics, 3rd edition, McGraw-Hill Inc., ISBN 0-07-027390-1, 1974

4 Hawksford, M.J. (Give reference to Track 1 of 'Unification' when known)

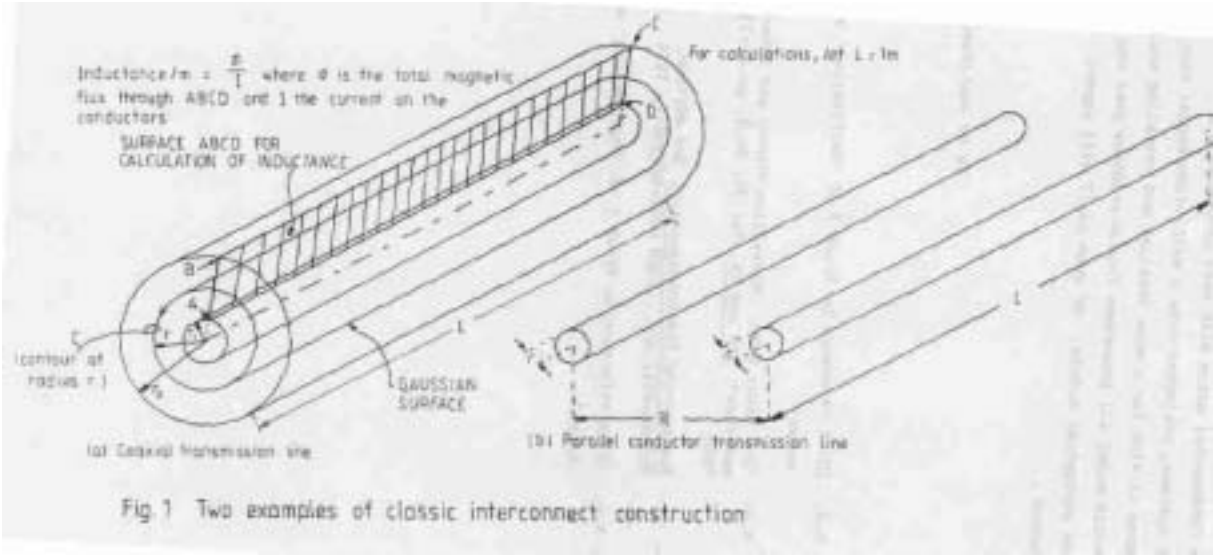

Fig 1 Two examples of classic interconnect construction

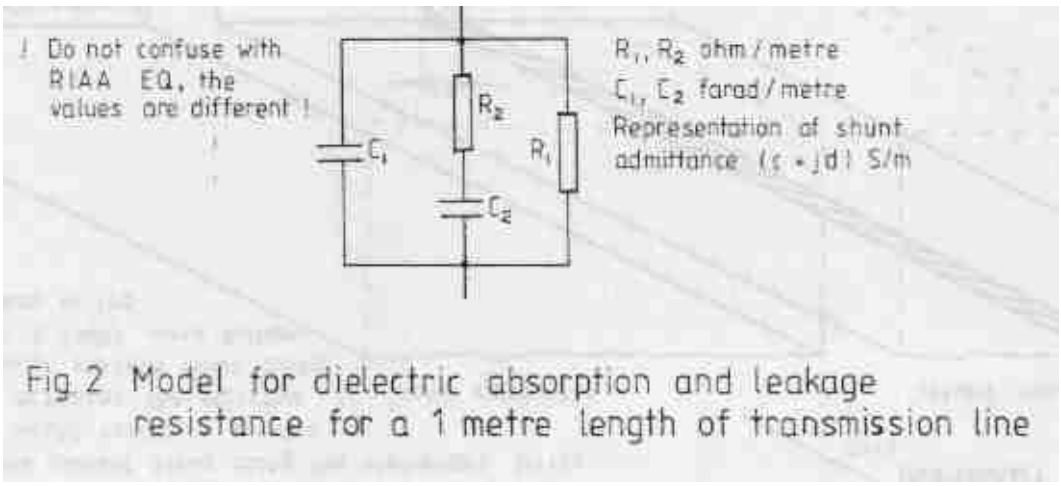

Fig 2 Model for dielectric absorption and leakage resistance for a 1 metre length of transmission line

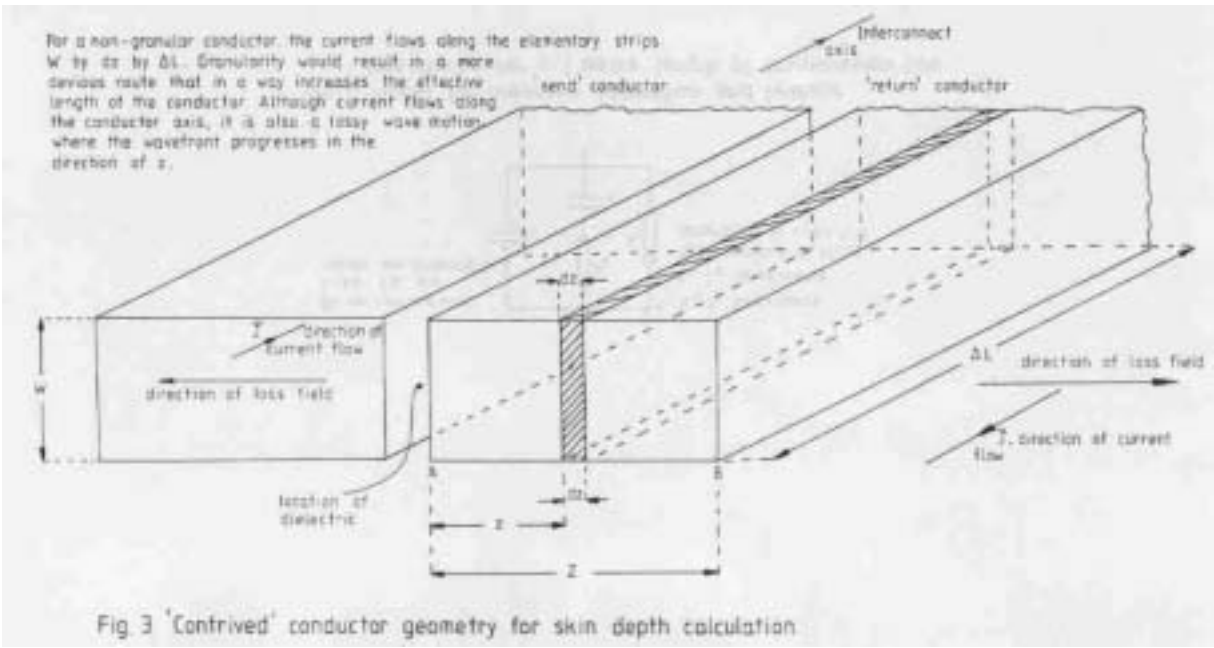

Fig 3 'Contrived' conductor geometry for skin depth calculation

The Essex Echo : Unification - Track 4

The aim of the Unification essays (1,2,3) has been to establish a deeper though personalised understanding of error mechanisms in audio systems by identifying that the underlying concepts exhibit a close empathy with transmission line theory and electromagnetism. This concluding track in the present series aims to show that the transfer-error function can incorporate the notions of transmission lines and, as such, forms a concise and accurate model of both the linear interconnect problem, including loudspeaker loading and the large area capacitor. We proceed by completing the mathematics to allow an efficient description of the transfer-error function and then open the concluding discussion to applications and observations of error interelationships.

The principle system to be analysed is shown in Fig. 1, where an amplifier with an output impedance Z_{out} drives an interconnect of length L metre which is terminated in a loudspeaker load Z_L. The analysis of the loudspeaker load was discussed on Track 1 (1), where a discrete data file, based upon an equivalent circuit of a Celestion SL600, has formed the reference impedance for the results to be presented. The driving impedance Z_{out} is topologically selected to be representative of a wide range of power amplifiers that can include, for example, the Quad 405.

Transfer-error function of interconnect

The non-ideality of a transfer function has been described (4,5) in terms of the transfer error function as,

$$E(f) = \frac{A(f)}{A_t(f)} - 1$$

where Fig. 2 illustrates a model of this function.

In the specific applications of audio interconnect, we shall represent the target function as "no cable" driven by a zero source impedance, whereby $A_t(f) = 1$. However, even a perfect cable must introduce time delay, consequently the complex form of the error function can be misleading. In order to emphasise the errors in amplitude response without the complications of phase, a modified function is introduced that is dependant upon the modulus of A(f), i.e.

$$E_m(f) = \frac{|A(f)|}{|A_t(f)|} - 1 = |A(f)| - 1$$

The transfer function of an audio interconnect, A(f), is derivable directly from the transmission line matrix equation that was developed in tracks 2 and 3 of this series (4,5), i.e.

$$\begin{bmatrix} V_1 \\ V_2 \end{bmatrix} = Z_0 \begin{bmatrix} \coth(\gamma L) & \operatorname{csch}(\gamma L) \\ \operatorname{csch}(\gamma L) & \coth(\gamma L) \end{bmatrix} \begin{bmatrix} I_1 \\ I_2 \end{bmatrix}$$

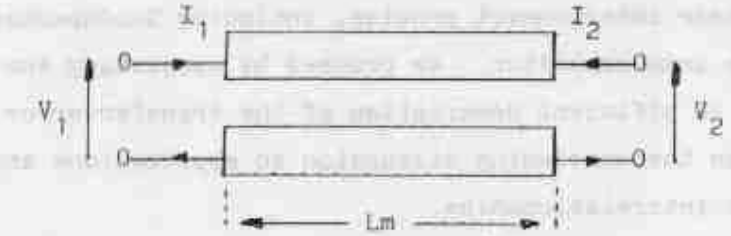

To facilitate the extraction of the transmission line transfer function, $A_\ell(f) = V_2/V_1$, the [Z] matrix is initially linearly transformed to a [h] matrix, where

$$\begin{bmatrix} V_1 \\ I_2 \end{bmatrix} = \begin{bmatrix} Z_0 \tanh(\gamma L) & \operatorname{sech}(\gamma L) \\ -\operatorname{sech}(\gamma L) & \dfrac{\tanh(\gamma L)}{Z_0} \end{bmatrix} \begin{bmatrix} I_1 \\ V_2 \end{bmatrix}$$

Noting that, $Z_{in} = \dfrac{V_1}{I_1}$ and $Z_L = \dfrac{-V_2}{I_2}$, then

$$\frac{V_2}{V_1} = \operatorname{csch}(\gamma L) \left[1 - \frac{Z_0}{Z_{in}} \tanh(\gamma L) \right]$$

(Note, for information, that the hyperbolic functions were listed in Appendix 2, Track 2 (λ))

Algebraic manipulation enables expressions for both Z_{in} and $A_\ell(f)$ to be derived, where

$$Z_{in} = Z_0 \left[\frac{Z_L \cosh(\gamma L) + Z_0 \sinh(\gamma L)}{Z_L \sinh(\gamma L) + Z_0 \cosh(\gamma L)} \right]$$

$$A_\ell(f) = \left[\cosh(\gamma L) + \frac{Z_0}{Z_L} \sinh(\gamma L) \right]^{-1}$$

To determine the overall system transfer function A(f), we note,(see Fig 1)

$$A(f) = \frac{V_1}{V_0} \cdot \frac{V_2}{V_1} = \frac{Z_{in}}{(Z_{in} + Z_{out})} \cdot A_\ell(f)$$

whereon substituting for $A_\ell(f)$ and Z_{in}, it follows

$$A(f) = \left[\left[1 + \frac{Z_{out}}{Z_L}\right]\cosh(\gamma L) + \left[\frac{Z_0}{Z_L} + \frac{Z_{out}}{Z_0}\right]\sinh(\gamma L)\right]^{-1}$$

The modified transfer-error function for $A_\ell(f) = 1$ is then simply,

$$E_m(f) = \left|\left[\left[1 + \frac{Z_{out}}{Z_L}\right]\cosh(\gamma L) + \left[\frac{Z_0}{Z_L} + \frac{Z_{out}}{Z_0}\right]\sinh(\gamma L)\right]^{-1}\right| - 1$$

The equations describing Z_{in}, $A_\ell(f)$, A(f) and $E_m(f)$ are actually completely general and can be used for any transmission line problem with the basic structure of Fig. 1, where the driving and load impedances Z_{out}, Z_L and the transmission line parameters [γ, Z_0, L] are determinate. In principle, the model is directly applicable to the loudspeaker interconnect, low-level interconnect and large area (one-dimensional) capacitor problems. I have embedded these equations in a computer program which when driven by the parameter set [a, b, c, d] (s,s) allows a straightforward and accurate method of analysis, that also includes skin depth where appropriate.

DIGRESSION

We will shortly present some example calculations based upon our model. However, as an interlude allow me a final digression to comment further as to the conceptual power of the transfer-error function as a description of linear distortion mechanisms:

Transfer-error function and multiple error structural representation

It is important to note that the transfer-error function attempts to present in a more sensitive way, the non-ideality in the system transfer function, where I am sure the methodology would have found sympathetic favour with our great grandfathers; because they lacked in sensitive instrumention their use of bridge techniques was prolific. In particular, the model of Fig. 2 shows the now familiar structure where the error is represented as a secondary signal which is superimposed upon the

primary signal - it is a logical method of visualising the system distortion. Since the transfer-error function is, in general, far from uniform the signal emanating from E(f) is highly coloured, as Martin Colloms' demonstrated to the AES in December. If this error signal is, say, in a range of ≈ -5→-50dB, it is capable in principle of implanting a sonic signature to the overall sound. However, if a particular error mechanism has a distinctive character that is describable by its individual transfer-error function, then this error may well remain audible even if more dominant errors exist, as such an error could be said to exhibit a degree of perceptual orthogonality. We are going to attempt to demonstrate how the basis for such a comment can be supported within a typical audio system. It should be noted, that in making this general comment, we refer more to the highly complicated and thus characteristic errors associated for example, with loudspeaker enclosures and drive units, where such errors can be subjectively described possibly as "wooden" or "metallic", i.e. the error mechanism has a characteristic sound. I personally believe this latter observation to be probable and is the mechanism by which a specific error source can be discriminated by a perceptive listener: though the source signal must itself be error free and not degraded, for example, by analogue tape recorder errors, as Angus Mckenzie constructively indicated during discussion time at Martin's AES lecture earlier this year.

Let us now give further consideration to the way multiple linear distortions combine within a system and see if there is a rationale for the suggestion that certain classes of individual error implant a distinct sonic characteristic.

Consider a system that is represented as a cascade of transfer functions A_0, A_1, A_2, ... A_N where the nominal target functions are defined A_{0t}, A_{1t}, A_{2t}, ... A_{Nt} (t → target). In other words A_0 is an approximation to A_{0t}, A_1 to A_{1t} etc. Fig. 3 illustrates the cascade together with the transfer-error function equivalent where the respective functions are E_0, E_1, E_2, ... E_N. For example, the system could represent the effect of an individual amplifier, a loudspeaker interconnect, an individual capacitor coupling network or any representative combination of error mechanisms.

The actual overall transfer function G_N may be expressed in two ways, (note the symbol $\prod$ infers a cascaded product, e.g. $\prod_{r=1}^{3} a_r = a_1 a_2 a_3$), i.e.

$$G_N = \prod_{r=0}^{N} A_r = \prod_{r=0}^{N} A_{rt} (1 + E_r)$$

where the overall target transfer function G_{NT} is,

$$G_{NT} = \prod_{r=0}^{N} A_{rt}$$

It is possible to define a transfer-error function E(N) for the composite system, as shown in Fig. 4, where,

$$E(N) = \frac{G_N}{G_{NT}} - 1$$

For a well-behaved system, $|\{E_r\}|_{r=0}^{N} << 1$, therefore products such as $E_0 E_1$ or $E_0 E_1 E_2$ etc. become very much less than the individual errors, these products in effect are the error of error terms.

Hence, to a good approximation, we may write

$$E(N) = \left[\frac{\prod_{r=0}^{N} A_{rt}(1 + E_r)}{\prod_{r=0}^{N} A_{rt}} \right] - 1$$

$$= \left[\prod_{r=0}^{N} (1 + E_r) \right] - 1$$

$$\therefore \quad E(N) \approx \sum_{r=0}^{N} E_r \quad , \quad \text{when } |\{E_r\}|_{r=0}^{N} << 1$$

[$\sum$ implies summation, e.g. $\sum_{r=1}^{3} a_r = a_1 + a_2 + a_3$]

That is, the transfer-error functions are combined, to a good approximation, by addition and NOT multiplication. Consequently the composite system may be modelled as shown in Fig. 5, IRRESPECTIVE OF WHERE THE INDIVIDUAL ERRORS APPEAR WITHIN THE AUDIO CHAIN.

Let us demonstrate this important observation by expanding E(N) for a simple example where $N = 2$, i.e.

$$E(2) = (1 + E_0)(1 + E_1) - 1$$

$$\therefore E(2) = 1 + E_0 + E_1 + E_0 E_1 - 1$$

$$\approx E_0 + E_1$$

PROVIDING both $|E_0|$, $|E_1|$ are sensible < 1 such that $|E_0 E_1| << 1$.

I personally believe that the structure shown in Fig. 5 gives a constructive insight into the mechanisms of linear distortion particularly as to a good approximation the lower-level errors are combined additively. It is therefore possible to appreciate more how the individual characteristics E_0, E_1 etc. combine and implant their signatures as the composite error is not substantially a convolution of the individual time-domain signals: each error signal maintains its identity without substantial modification from other error sources in the cascade.

We observe, therefore, that as the system complexity is advanced, the array of individual errors proliferate to form a fuzzy residual or veiling of the source signal: it is analogous to the observation of a visual image transmitted through multiple layers of lightly patterned or low quality glass panes. The old adage, "the wider you open the window the more the muck comes through", is actually a hindrance (i.e. it makes you want to close the window!) to modern system development and does not relate to well-tuned systems - especially as the objectionable muck appears to reside on the system windows that define the individual error mechanisms. The additive model therefore complements Harry Pearson's discussion on transparency (12) and gives us an objective picture of the subjectivist's notion of "removing veils". Each transfer-error function is an individual veil. I hope the veils are now beginning to clear from my arguments - as they are in Marrakech.

END OF DIGRESSION

Loudspeaker interconnect example errors

OK, let us now illustrate these observations with some examples of loudspeaker-interconnect errors based upon the theory we have developed. The following table shows four interconnect examples of differing loop resistance, loop inductance, capacitance and conductor effective radius (Z). The figures quoted are for 10m lengths of interconnect.

If we assume $e_r = 2$ (relative permittivity) then the static inductance and capacitance (per metre) are linked by $LC = 2.224.10^{-17}$ HF/m2, (see track 3 (s))

INTERCONNECT DATA BASE: L = 10m

Example 0:	C	= 1000pF/m	Example 1:	C	= 1000pF/m
	L	= 22.2 nH/m		L	= 22.2nH/m
	R_{int}	= 10 mΩ/loop metre		R_{int}	= 10mΩ/loop metre
	Z	= 0.05mm (litz)		Z	= 1mm (solid core)
Example 2:	C	= 20pF/m	Example 3:	C	= 20pF/m
	L	= 1.11μH/m		L	= 1.11μH/m
	R_{int}	= 10mΩ/loop metre		R_{int}	= 10mΩ/loop metre
	Z	= 0.05mm (litz)		Z	= 1mm (solid core)

KEY: C, static capacitance/m R_{int}, dc loop resistance/m
L, static inductance/m Z, effective conductor radius

(capacitance and dc resistance values have their origins in Martin's table (6), inductances are calculated assuming ϵ_r=2 and effective conductor radii are invented for illustrations)

In Figs. 6-9, four groups of results are presented for each of the four interconnect examples. The results show plots of the modified transfer-error function $E_m(f)$ over a frequency band 10Hz to 100kHz. The four groups which refer respectively to the choice of source and load impedances are defined:

Group 1: Z_L = 4Ω, Z_{out} = 0Ω
Group 2: Z_L = 4Ω, Z_{out} = (0.05Ω in series with 4μH)//100Ω
Group 3: Z_L => SL600, Z_{out} = 0Ω
Group 4: Z_L => SL600, Z_{out} = (0.05Ω in series with 4μH)//100Ω

The computed results presented in fig. 6-9 are as follows:

(insert Fig. 6)

Fig. 6 Cable example 0, group 1
Cable example 1, group 1
Cable example 2, group 1
Cable example 3, group 1

(insert Fig. 7)

Fig. 7 Cable example 0, group 2
Cable example 1, group 2
Cable example 2, group 2
Cable example 3, group 2

(insert Fig. 8a)

Fig. 8a Cable example 0, group 3
Cable example 0, group 4

(insert Fig. 8b)

Fig. 8b Cable example 1, group 3
Cable example 1, group 4

7a

(insert Fig. 9a)

Fig. 9a Cable example 2, group 3
Cable example 2, group 4

(insert Fig. 9b)

Fig. 9b Cable example 3, group 3
Cable example 3, group 4

Although the frequency range has been deliberately set to represent the audio band, the computer model can accommodate a wider range. Though this is more of academic interest, amplifiers still operate over a wider bandwidth where hf behaviour in conjunction with non-linear mechanisms and hf interference may well be of concern. In Fig. 10, six computer results are presented for cable examples 0 and 1 each with respective loads 4.712Ω, 10Ω and 10kΩ//200pF (the former representing an approximation to the hf characteristics impedance).

The selected bandwidth is 1kHz to 30MHz. Fig. 10a demonstrates that an interconnect with minimal skin depth exhibits virtually perfect behaviour, while solid core shows a predictably greater hf loss. For both traces, wave effects can just be observed in the 1MHz to 30MHz region, though the matched impedance minimises the standing wave patterns. The non-matched interconnect in Fig. 10(b) yeilds a greater standing wave pattern. Interestingly, in Fig. 10(c), the 10 metre interconnect when loaded by 10kΩ//200pF still shows a non-ideal error behaviour though the losses in the audio spectrum are of a much lower order, where again the solid core conductor yeilds the greater loss. However, it would appear from a purely linear analysis, that for this latter example, the level of errors are only of academic interest. It is therefore reasonable to conclude that if low-level interconnects operating with relatively high load impedances adversely affect sonic performance, that signal dependant factors are at work and we must look, for example, to the distributed diode/capacitor/resistor networks offered by Kamada of Hitachi(7,8).

The results presented in Figs. 6-9 demonstrate the error in amplitude response introduced by the interaction of amplifier impedance,

interconnect parameters and a complex loudspeaker load. At low frequency, the results are predominantly determined by the resistive properties of the conductors, but at higher frequency both inductance due to the external field and the impedance of the conductor due to the internal conductor loss field start to dominate. The error voltage across the cable is a function of the loudspeaker load current; consequently an image of the loudspeaker load impedance is mapped on to the overall transfer-error function as is readily observed by the graphs. In our example, we assume a linear though complex loudspeaker load impedance. In practice, this is not exactly the case: the loudspeaker impedance is itself an image of all the mechanical and acoustical parameters within the loudspeaker system including stored energy and non-linear contributions from non-linearity in [Bl] for each drive unit. In truth it is an intricate picture that is often grossly simplified by too insensitive measurement practice.

Even our somewhat simplified results (to be fair, they are a very close first-order, linear approximation) show significant vestiges of error that are particularly prevalent in the mid band and at high frequency. It is no wonder that different cable constructions lead to differing subjective performance, though carefully observe the importance of including both interconnect and system in the assessment.

Another important observation is that due to component tolerances and variations in drive-unit parameters, the errors will be different on each channel of a stereo system, particularly where there are 'high-Q' resonances of slightly differing centre frequency. Also, once non-linear elements are introduced and combined with the fact that each stereo loudspeaker is in a different dynamic state (due to the presence of stereo information), then the actual error from each loudspeaker will be subtly different, that will not follow the signal clues necessary to form optimum stereo perception. The stereo stage is diluted and the individual channel errors draw attention to each loudspeaker, complementing the observation that system errors often cause changes in dimensionality. Ideally, if we could audition the individual channel errors in stereo, this observation would be more apparent. In fact, an interesting experiment would be to use two differential amplifiers to monitor the error signal across each interconnect of a stereo system, make a stereo recording using PCM F1

and then replay the error in stereo for subjective appraisal. This would enable both a subjective assessment of the error signal as well as an estimate of the stereo information. The same concept is applicable to John Curl's and Martin Colloms' capacitor error test. This method should become an integral technique within loudspeaker interconnect assessment and compares with my earlier suggestion (5) for auditioning loudspeaker enclosure errors.

I feel these observations to be important, as it is generally believed that the resolution of system errors are best observed in stereo where the impact upon transparency, dimensionality and dynamic and transient integrity is more apparent. A subjective monitoring environment must embody all the perceptual clues available for fine resolution to be achievable. Small differential channel errors in frequency response represent relatively large differential channel errors in transfer-error function. I have read with interest the recent letter by Dr Lesurf (9) who appears to agree with me in this area, I thank him for his comments.

Measurement of conductor internal loss wave (skin depth) in the time domain

As a final observation of skin depth phenomena and to substantiate my original claim (8) that the internal propagating fields, that are directed along the radius represent a lossy energy reservoir that time smear a small fraction of the applied signal, I will present some measurements and computer simulation of this phenomena. Note my claim that, for a conductor operating in a skin depth limited region ($\delta < Z$), is that the time dispersion is significant, though the error is at low level. I previously suggested (8), that if a tone burst of current was passed through a conductor, when the tone was switched off, the internal propagating loss wave would have to dissipate before the error voltage across the conductor was zero, as the loss wave is effectively temporary stored energy.

For the experiment, a multi-strand steel conductor of 2.6mm diameter was used. A thin heat shrink sleeve was placed over half its length and the cable then folded symmetrical to form a short circuit, parallel interconnect with minimal dielectric space between conductors. Finally, a larger heat shrink sleeve was placed over the whole cable to hold the conductors tightly together, again to minimise the enclosed area, by keeping the parallel conductors in close proximity.

The purpose of the construction was two-fold:

(i) steel being magnetic, the skin depth effects are exaggerated as δ is a function of μ (hence my dislike of steel pipes)

(ii) the close conductor spacing reduces the external magnetic field, i.e. loop inductance, thus reducing the error voltage due to $L_e \frac{di}{dt}$

Even with the precaution (ii), there is still an error due to the changing external magnetic field, $L_e \frac{di}{dt}$ which is superimposed upon the error waveform across the conductor due to the internal loss wave. This component must be subtracted to expose the desired error. The circuit shown in Fig. 11 was constructed where an integrator enabled a signal proportion to $\frac{di}{dt}$ to be extracted. A dual plug-in oscilloscope with a differencing facility allowed the proportion of the error waveform due to the changing external magnetic field to be subtracted. The internal field error residue is then displayed.

The circuit of Fig. 11 uses two operational amplifiers, where the overall feedback, with some input compensation, attempts to produce a good replica of the tone burst generator output waveform. This signal then drives a transconductance amplifier to feed a tone burst of current into the conductor under test. However, even if the output wave (at A) is slightly distorted, this is of no consequence as the second operational amplifier forms an accurate integrator. Hence the input to the integrator must be the differential of the output - which is just what we desire, i.e. a component proportional to, $L_e \frac{di}{dt}$. The integrator remains dc stable as there is overall dc negative feedback via the first operational amplifier, but there is no local dc feedback on the actual integrator (between B and A), hence wide-band integration.

Fig.12a shows the measured output trace when the external field contribution is nulled, alongside the input tone burst measured at point A (Fig. 11). The tone frequency is 1 kHz.

Fig.12b illustrates a tone burst that is modified by a computer, programmed to model the skin depth effect (conductor operating in a pure skin depth limited region). Effectively the tone burst was synthesised using a truncated Fourier series (20 harmonics), where each component was modified by a +3dB/octave slope and $+45^{\circ}$ phase shift filter, which represents the internal wave in a non-granular conductor (see Track 3 (3)). Although the example is rather contrived, the results of measurement and theory are in close harmony and I hope they demonstrate my original prediction of a time dispersive error signal, where the dispersion is significant, though of low level. In

making this observation, I would like to clarify any misunderstanding that some observers have expressed! The component which is dispersed is the error component across the conductor that results from the internal loss wave that propagates (diffuses) radially and defines the current density along the conductor axis. The primary signal is not itself time dispersed to the same extent; the velocity of propagation is high within the dielectric and it is not until high frequency that reflection phenomena are exposed, observation of the interconnect, transfer, error function plots in Fig. 10 should support this comment.

It is interesting to observe how a filter with a 3dB/octave slope modifies the input waveform where we see considerable time differences. Note also how two cycles of the input tone burst become 2.25 cycles (of error) within the same time slot (- an apparent increase in pitch?). Though a more usual filter with a 6dB/octave slope (i.e. a differentiator) introduces a greater amplitude error, there is less time dispersion. It should also be noted that when a wire operates in a purely skin depth limited region, the time dispersion is proportional to the tone burst frequency, thus if the tone burst frequency was 10kHz, the apparent shape of the error waveform in Fig. 12 would remain unchanged, though, of course, the time scale and amplitude would be different.

Finally, while on the subject of tone burst errors in steel conductors, an effect I hope Martin will like: I conjectured that if a reasonably powerful magnet is brought into close proximity to the conductor, it will modify both the current distribution and μ_r within the conductor and thus influence the error signal. During observation of the internal field error waveform, we attempted this experiment using a loudspeaker magnet (what else?) and to our pleasure there was a change in the error level; it was only just perceptible but nevertheless observable - an interesting aside.

This discussion has attempted to demonstrate more formally the distortion mechanisms that are present at equipment interfaces, where together we have observed the dependance upon L, C, $Z_{int}(Z)$, Z_{out} and Z_L by using a relatively general purpose transmission-line model. It should be noted, however, that in a practical system both the load and source impedances may be partially non-linear, the first being a reflection of drive unit non-ideality and inductor saturation while the latter, an image of amplifier misbehaviour which modulates Z_{out} dynamically, a distortion

mechaniam often termed amplifier interface distortion.

Another area worthy of future research is inter-equipment interference which is often injected into electronic apparatus via the numerous mains input ports. Many power supplies are relatively transparent to such interference, which can span a bandwidth of many megahertz. Consequently wide-band interference will propagate along the audio interconnects and be injected into sensitive amplifier stages that may well exhibit poor signal handling ability at hf. Our results on interconnect performance demonstrate that there are different hf characteristics that are a function of length, geometry, conductor diameter (solid core or litz) and load and source impedances. Consequently, changing a length of mains-lead or a conductor diameter, for example, which is not necessarily matched to the "house wiring", will inevitably alter the hf transmission characteristics. Also, digital equipment such as compact disc players are excellent sources of wide band radio interference. Try operating a radio (fm should be OK) in close proximity to a player, and hear what happens. David Frakel recently gave me a convincing demonstration of this phenomena in conjunction with a top-rate CD player and tuner.

I am therefore of the conviction that, though appreciated in engineering circles, this area is neglected with respect to audio performance in an objective sense, specifically as it relates closely to the more measurable characteristics of cables. Possibly an ensemble of audio equipment should be objectively assessed as a complete system that includes electronics, transducers and interconnects, rather than individual components under laboratory conditions. But then earth loops and interference may make the results inaccurate, that change with time of day, preventing the true performance from being discovered ... in this sense the subjectivists have got it right: they listen to everything, warts and all!

Capacitor models and wave propagation

A capacitor is constructed of two conducting plates separated by a dielectric as described in track 3 ( ). In this discussion, we shall assume this structure to be relatively long compared with the width, and that the parallel plates are driven uniformly across the width on one end only. Consequently, the capacitor is a one-dimensional, open-circuit transmission line, where the electrical terminal behaviour is described in the linear sense by the transmission line matrix equation. Observing the matrix equation, the input impedance is then determined when $I_2 = 0$ as,

$$Z_{in} = \left.\frac{V_1}{I_1}\right|_{I_2=0} = Z_0 \coth(\gamma L) = \left.\frac{Z_0}{\gamma L}\right|_{\text{at low frequency}}$$

This equation is much simpler than those derived from cascaded lumped RLC networks!

The principal electrical difference between an interconnect and a capacitor is the characteristic impedance. An interconnect generally has a characteristic impedance ranging between 2Ω and 300 Ω, while a capacitor has a characteristic impedance that is a small fraction of 1 ohm (see later examples).

However, a capacitor's performance is determined both by its internal electrical behaviour and the external parasitic elements of lead resistance R_{lead} and lead inductance L_{lead}. The effect of these parasitic elements is best appreciated by reference to the equivalent series RLC circuit shown in Fig. 13a. The circuit reveals the classic capacitor behaviour of a falling 6dB/octave impedance at lf, followed by a damped resonance and a rising 6dB/octave curve due to the series inductance. Even though lead inductance is only 10s of nano henry, it still dominates the hf region as the impedance of C falls to a very low value determined by its characteristic impedance. If you now refer to Ben Duncan's July 1986 article (page 43), various families of impedance curves are presented that are reminiscent of the behaviour of the circuit of Fig. 13a assuming appropriate selection of R_L and C.

However, a more detailed observation of Ben's Fig 25a, particularly curve 3, reveals a response between 1kHz and 10kHz that is not predicted by the basic model, similar characteristics can also be found in capacitor data books.

To account for the impedance slope that approximates to -3dB/octave, the more general transmission line model of Fig. 13b is required. Although at audio frequencies the plate dimensions of an electrolytic capacitor (several metres) is still not sufficient to exhibit standing wave effects, the resistance/metre of each plate is relatively high due to small thickness.

As a result, there is a tendency for the effective plate length to diminish with increasing frequency causing the capacitor impedance to fall at ≈3dB/octave and not 6dB/octave. It is possibly easier to visualise the capacitor as a cascade of RC networks as shown in Fig. 13c, though, of course, in the limit, the network becomes distributive. However, by applying the transmission line equation there is no approximation, where the total impedance of the capacitor is given by,

$$Z_{cap} = R_{lead} + j\omega L_{lead} + Z_0 \coth(\gamma L).$$ (see Track 2, p.37, column 2 for Z_0, γ)

To illustrate the workings of the capacitor based upon this equation, Fig. 14 presents a series of computer results for the following data:

capacitor plate length = 10m	capacitor plate width = 0.05m
dielectric thickness = 0.1μm	dielectric constant = 10
plate conductivity = $5.8.10^7$ s/m	total static capacitance = 442.7μF
capacitance/metre = 44.27μF	inductance/metre = 2.51nH/m
plate resistance/metre = 0.021Ω/m	$\sqrt{L/C}$ = 2.38 mΩ

Fig.14(a) Capacitor with unrealistic plate thickness of 10cm, $R_{lead} = 0\Omega$ and $L_{lead} = 0H$ (plates assumed litz, no skin depth)
Fig.14(b) As in (a) but plate thickness = 0.05 mm (more realistic)
Fig.14(c) As in (b) but $R_{lead} = 0.05\Omega$, $L_{lead} = 80nH$

Although the capacitor is an open-circuit transmission line, the conductor resistance is sufficiently high that all standing wave patterns are always attenuated at hf. This observation is illustrated in Fig. 14a and b, where unrealistic plate dimensions are required to show any standing wave residuals. Consequently, in a practical capacitor, lead inductance dominates at high frequency yielding the characteristic 6dB/octave impedance curve. This characteristic will continue until the wires connected to the capacitor themselves show transmission line effects. However, further scrutiny of Fig. 14b reveals an impedance region of -3dB/octave, it is here that the effective plate dimension is reducing due to the distributed RC networks of Fig. 13c, the longer the capacitor plate, the more serious is this problem as the transition frequency from -6dB/octave to -3dB/octave is lowered. If we now include lead resistance and lead inductance, the result of Fig. 14c is predicted, which can be reasonably compared in general shape to Ben Duncan's Fig. 25a, curve 3.

Corollary

It is interesting to observe that these results predict the existence of a new passive component. Imagine a capacitor plate is etched so that the

plate width is extremely narrow and the plate length extremely long; the new etched plate forms a narrow path that winds its way back and forth across the conductor surface. Such a device would offer a wide frequency band where the impedance falls at 3dB/octave (phase -45^{o}). Our new component would have a wide application in analogue filter design and could be used, for example, in the frequency shaping filter required within a pink noise generator. Also, by varying the width of the conductor using selective etching of the plates, the impedance characteristic could be programmed at manufacture to give a more general form. In Fig. 14d, an impedance curve is presented for a modified capacitor designed to the following data:

effective plate length = 500m	effective plate width = 1mm
dielectric constant = 10	dielectric thickness = 0.1μm
plate thickness = 0.05mm	plate conductivity = $5.8.10^{7}$ S/m
static capacitance = 442.7μF	lead resistance = 0.05Ω
lead inductance = 80nH	

Observe the large -3dB/octave region from 2Hz to 200 kHz. Such a device could be called a C-DIFFUSOR and represents the operation $1/(D\sqrt{j\omega})$ where D is the C-Diffusor constant.

Observations on capacitor construction

The one-dimensional analysis demonstrates that the shorter the length of the plate, the less problematic is the effect of plate resistance as the "-3dB/octave region" is positioned relatively high in frequency. The solution to the design of large value capacitors is therefore apparent: the capacitor should be constructed from a parallel connection of small area capacitors, where the connections are made at two nodes only. Two example structures are shown in Fig. 15.

Some audio designers (including myself) have already used this principle by paralleling arrays of low valued capacitors. Such a technique lowers the effective series resistance, lowers the effective series inductance and by using smaller area capacitors, a composite is achieved that operates closer to the theoretical ideal over a much wider bandwidth. The maintenance of a well-behaved high frequency performance is extremely important particularly in class AB power amplifiers, where the reservoirs are loaded by transient currents that are non-linearly related to the primary audio signal and can exhibit bandwidths way in excess of the audio band. It is also important that paralleled components are connected to only two circuit nodes, otherwise quite complex RLC structures are created that will impair hf performance. Possibly in a more ideal world, litz wire would be used in power supply lines, where the individual strands would terminate on the individual (small) plates of a parallel assembly of capacitors. The increased conductor diameter would help reduce overall lead inductance, while the fine strands of litz would eliminate skin depth problems particularly at hf.

At an academic level, I am personally fascinated by the duality between skin depth in conductors, which is essentially a distributed LR network, and the distributed effect of RC in long capacitors. The first gives a rising impedance of 3dB/octave (phase 45^{o}) while the latter gives -3dB/octave (phase -45^{o}), when the effects are considered in isolation. Both phenomena are described by the transmission line equation and can therefore be considered as wave effects. I know some engineers prefer to use a more restrictive definition of a wave phenomena, nevertheless, the generalised equationswe have developed apply to all cases, therefore the semantics are of little relevance.

I certainly feel that Dennis Morecroft in his pioneering capacitor research is on a constructive route, though I would suggest that his comments on circulating currents result from the capacitor plates and dielectric operating as a two-dimensional transmission line, where interfering wave patterns and multiple boundaries give rise to a more intricate surface current distribution. The slits introduced into the plates partially limit the current distribution by forcing a preferred direction to the lossy wave propagation that is more akin to a one-dimensional transmission line. Clearly if the slits were orientated along the width, we would expect a degradation in performance as the effective plate length is increased leading to an increase in the sub -6dB/octave impedance region. This comment supports the observation by Dennis that there is a preferred alignment to the slit pattern.

The objective of capacitor design is to maximise the region over which the -6dB/octave impedance region operates. Though, in practice, coiled capacitors have multiple taps, the tap positions appear somewhat empirical and do not directly address the central problem. Multi-layer, parallel constructions are clearly a solution, though equally the "quality" of plate conductor, electrical bonding of lead-in wires, dielectric type and mechanical damping are paramount. To anticipate a multi-layer construction, using LC-OFC plates with integral, litz conductors where each strand is an extension of the plate material,could prove a most interesting device.

The area which I have not included in the discussion is the effect of conductor surface etching and variation in dielectric thickness over a large area. Surface etching forms a fractal pattern that effectively increases the surface area as the area integrated over the valleys and hills is greater than the plain, the capacitance therefore increases but at the expense of minute dimensional variations of the dielectric thickness. Any geometric irregularities must inevitably affect the impedance profile particularly in, or close to, the "-3dB/octave region". Couple this with dynamic modulation of plate dimensions with applied voltage and further sources of

error are unveiled. I am sure these effects are relatively small but perceptive listeners indicate there are problems, so I, for one, will keep an open mind.

We therefore observe a strong similarity between an audio interconnect and a classic, large-area plate capacitor, where the fundamental differences are principally only one of dimension. Regrettably, this similarity is also an Achilles' heel as the performance of the capacitor is inevitably degraded by the signal current that flows in the longitudinal direction of the plates, where I suggest that ideally, the current flow should be substantially transverse as typified by the structures of Fig. 15. This leads directly to a more theoretic capacitor by minimising the effects of conductor resistance and of the associated irregularities in dielectric dimension. The time delay caused by the diffusion of charge along the conductor surface is therefore minimised and the "-3dB/octave" region correspondingly eliminated. If we observe the duality of voltage and current in comparing inductors and capacitors, then the error due to charge diffusion yields a similar result to that shown in Fig. 12, we have turned full circle. Since in principle a new device that is based upon a solid core wire can be configured to give an impedance proportional to $\sqrt{j\omega}$, we designate this device an L-DIFFUSOR, which is the dual of the C-DIFFUSOR. However, the L-DIFFUSOR is less practical due to the contribution of the external magnetic field, the only practical method is to construct a capacitor with "thick plates" ... but that has problems of Skin! However, the C-DIFFUSOR with etched plates would appear to be feasible and be an adaptation of present-day capacitor design.

We therefore conclude that by forcing the "3dB octave region" higher in frequency by using a parallel construction of smaller area plates, the dynamic range, bandwidth and minimum impedance of the capacitor is greatly enhanced. To take full advantage of this effect, particularly in reservoir capacitors, conductors must be of substantial diameter to lower lead inductance. Unfortunately, the internal fields then yield skin depth effects at hf, again bounding the hf impedance, hence capacitor leads should be of large diameter, litz construction, ideally with each strand of the litz wire terminated on an individual plate. Consequently, the common node where strands are ultimately combined can be optimally placed within the circuit structure and, as a bonus, the parallel structure will also minimise performance dependance on fractal surface irregularity.

A final comment on characteristic impedance

In the literature on cables, the characteristic impedance is often quoted as a real number, for example 50Ω or 75Ω. This figure is applicable when the signal frequency is sufficiently high that the inductance and capacitance dominate the expression for Z_0, whereby from our earlier expression for the characteristic impedance it follows,

$$Z_0 = \left[\frac{L_e}{C_e}\right]^{0.5}$$

series inductance and shunt capacitance dominate

However, at audio frequencies this is simply not true and the more general complex impedance for Z_0 must be used - an expression where the conductor resistance dominates over the inductive reactance. Consequently the idea of using a transmission line fed from say 75Ω and terminated in 75Ω (Z_0 = 75Ω at hf) is unfounded as an evaluation of Z_0 will reveal, even though matching is advantageous (see Fig. 10) at hf.

I am also concerned by some of the figures quoted for loop inductance when interconnects are reviewed. They do not always agree with the theory $L_e C_e = \epsilon\mu$ (though note my earlier comments in Track 3 on measuring the actual effective length and on coiled conductors. If an inductance bridge operating at, say, 1kHz is used to measure loop inductance, my own measurements reveal the short-circuit loop impedance is nearly resistive, therefore the bridge reading is often grossly distorted (unless both resistance and inductive reactance are balanced, but note $\omega L_e < R$). If some of the published values for L_e H/m and C_e F/m are substituted into $\epsilon_r = L_e C_e/(\mu_r \mu_o \epsilon_o)$, then some rather strange dielectric constants appear (note there is far less problem in measuring C_e over short, open-circuit cable runs). Therefore, I am highly sceptical on the figures often quoted for loop inductance, and I would also suggest the figures stated for Z_0 are a nonsense at low frequency.

Conclusion

The four essays in this series have discussed in some depth the concepts of transmission line systems. The approach has been rigorous, yet I trust the results are accessible, where a principle objective has been to demonstrate that the more general case solution adds only marginal computational complexity over the approximate lumped networks (see Appendix).

Our methodology has attempted to unify several aspects of our subject by illustrating that wave propagation is the basic concept of a range of error mechanisms, including the large area electrolytic capacitor currently being researched by Dennis Morecroft of DNM. The techniques presented have by necessity been linear, though where non-linear mechanisms intrude, this has been indicated.

The essays have extended the work of the original Essex Echo on interconnects both with respect to Electromagnetic Theory and its relationship to wave propagation, both external and internal, to the guiding conductors. I trust the experimental and computer results, particularly on skin-depth phenomena, will help clarify and substantiate this earlier work. Also, the discussions have focussed on the application of the transfer-error function which has formed continuity with my earlier expositions. In particular, I feel the emphasis on the additive rather than the multiplicative assembly of multiple error sources is paramount: errors are compounded essentailly by superposition rather than convolution in the time domain and therefore exhibit a greater probability of maintaining their individual sonic identities. Note how this observation is apparently lost when we observe only a cascade of transfer functions, which combine multiplicatively.

The extensions to incorporate non-linear mechanisms together with wave propagation principles is an interesting, though daunting prospect for future research, where it would seem important for the non-linear processes to be decoupled from memory effects, i.e. distortion that is aperiodic, together with a simple and smooth characteristic (hence my dislike of high overall negative feedback where the distortion characteristic always depends upon the history of the signal).

My concluding rumourings on non-linearity stem from the instinctive belief that the work on interconnects is far from complete, where there remains a performance regime barely touched upon by linear analysis that can introduce a form of transient distortion. This doubt arises in part by the work on interconnects by Kamada, Martin Colloms, Dennis Morecroft and Van den Hul, and in part by my recent French experience (see Track 1). My knowledge of interconnect performance is still, I admit, only in its infancy. It is true we can predict the transfer-error function for

an arbitrary and complex load impedance, terminating an interconnect of arbitrary length, over a very wide frequency band, and it is true the resulting errors, especially for the loudspeaker load, are undesirable in the extreme. Yet my instinct focuses upon parametric changes in the performance of electronics with differing interconnects, conductor granularity, boundary effects, potential barriers and embedded directionality; the true domains of fuzzy distortion. Remember, measurements performed within the steady state imply long-term averaging (usually several cycles) and the signals are generally of substantial level - music is instant by instant where the transient events are of short duration and remember Fourier only applies in the purely linear regime. However, these subjects are not for today, and I promised to stay in the world of acceptable concepts, at least for 1985. So these thoughts will be stored for a future occasion.

Finally the time of writing (most of these essays) is Christmas Eve 1985, there is not a Christmas tree in sight and the sun in Marrakech has shone all day from a typically cloudless, blue African sky. The say in Bab j Did that every interconnect should have a silver lining ... Good stuff, eh Martin? Tomorrow, I shall design a new unity-gain, Pontoon power amplifier (||).

Bon Annee!

Acknowledgement

I would like to thank Paul Mills of Audio Research Group, Essex University for his help in preparing the impedance values of the Celestion SL600 from Computer models. My thanks also to Graham Bank and Ed Form for allowing access to passive crossover component values used in the SL600 and for permission to use the SL600 as a loudspeaker example in the simulation plots.

1. Hawksford, M.J., 'The Essex Echo: Unification Track 1', HFN/RR, Vol. 31, No. 5, pp. 53-59, May 1986.

2. Hawksford, M.J., 'The Essex Echo: Unification Track 2', HFN/RR, Vol. 31, No. 8, pp. 33-39, August 1986.

3. Hawksford, M.J., 'The Essex Echo: Unification Track 3',

4. Hawksford, M.J., 'The Essex Echo: on errors, low feedback and fuzzy distortion', HFN/RR, Vol. 29, No. 9, pp.37-41, September 1984.

5. Hawksford, M.J., 'The Essex Echo: Reflexions', HFN/RR, Vol 30, No. 12, pp. 35-40, December 1985.

6. Colloms, M., 'Cable controversies', HFN/RR, Vol 31, No. 5, pp. 47-63, April 1984.

7. Kamada, 'Statistical and legitimate analysis of sound quality of LC-OFC audio cable and plug connector', Hitachi Cable Ltd, Tokyo, Japan, August 1985.

8. Kamada, O, 'Theory of audio cable evolution', Face-to-face talk between Saburo Egawa (critic) and Osao Kamada, (Inventor of LC-OFC), Hitachi Cable Ltd, Tokyo, Japan.

9. Lesurf, J.C.G., Letter to the editor, HFN/RR, Vol.31, No. 7, p.27, July 1986.

10. Hawksford, M.J., 'The Essex Echo: Maxwellian theory and interconnect memories, HFN/RR, Vol. 31, No. 8, pp. 27-33, August 1985.

11. Hawksford, M.J., 'Pontoon amplifier construction incorporating error-feedback location of floating supplies', 78th Convention of the AES, preprint 2247 (A-14), May 1985.

12. Pearson, H., "The second American audio revolution", HFN/RR, Vol.31, No.1, pp.37-39, January 1986

APPENDIX

First-order lumped element networks

To approximate the generalised transmission line model into the lumped element network more commonly associated with audio interconnects, consider the overall transfer function A(f) of the system in Fig. 1, when $|\gamma L|<1$. The first-order approximation follows by truncating the series expansions for cosh (γL) and sinh (γL) to contain no terms higher than γL, i.e.

$$\cosh(\gamma L) = 1 \quad , \quad \sinh(\gamma L) = \gamma L$$

Substitution reveals the approximate transfer function $A_\ell(f)$,

$$A_\ell(f) = \left[1 + \frac{Z_{out}}{Z_L} + \left[\frac{Z_0}{Z_L} + \frac{Z_{out}}{Z_0} \right] \gamma L \right]^{-1} \qquad (2)$$

Noting the relationships of γ and Z_0 to {a, b, c, d} , then

$$A'_\ell(f) = \left[1 + \frac{Z_{out}}{Z_L} + \frac{(a + jb)L}{Z_L} + Z_{out}\,(c + jd)L \right]^{-1}$$

The transfer function $A'_\ell(f)$ describes exactly V_2/V_0 for the lumped-element network shown in Fig. A1. The first-order network is shown for completeness, though I would suggest that the more general expression $A_\ell(f)$ is sufficiently computationally accessible to make approximation unnecessary, especially as the approximation loses the effect of propagation.

However, the full transmission line model is still required to represent the internal fields of the conductors, where the expression for $Z_{int}(Z)$, discussed on Track 3, is embedded in the elements a, b. If the network of Fig. A1 is analysed, you should observe complete agreement with the expression $A_\ell(f) = V_2/V_0$: general transmission line theory is compatible with the lumped-element approximation, though the sphere of application of the latter is bounded.

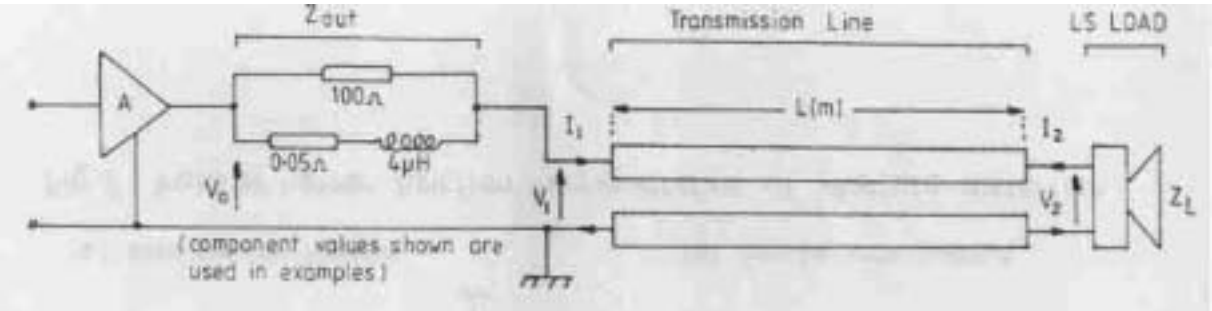

Fig. 1 Amplifier / interconnect / loudspeaker under investigation

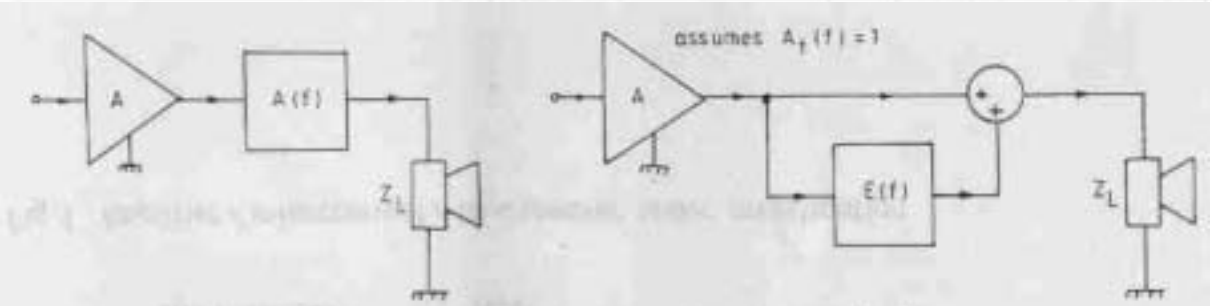

Fig. 2 Transfer-error function representation of interface distortion

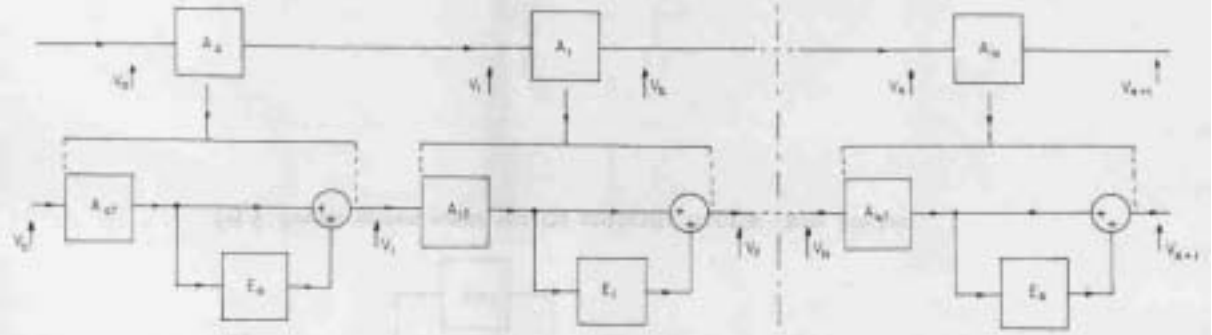

Fig. 3 Representation of a series connection of transfer functions, A_0 A_1 ..... A_N

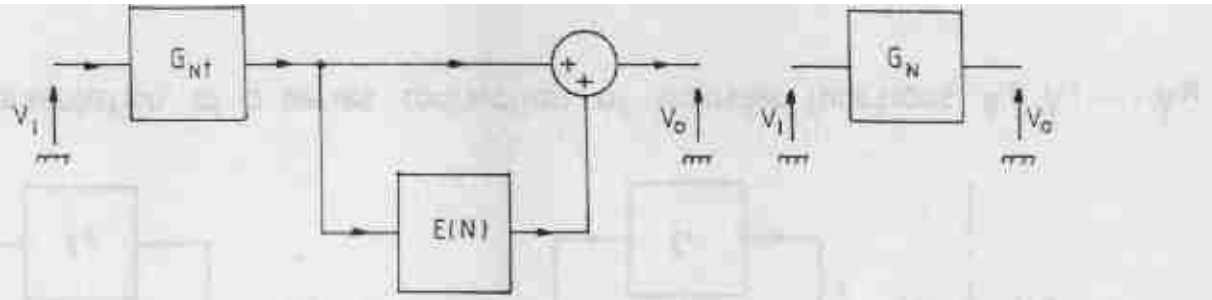

Fig. 4 Overall system model showing composite transfer-error function

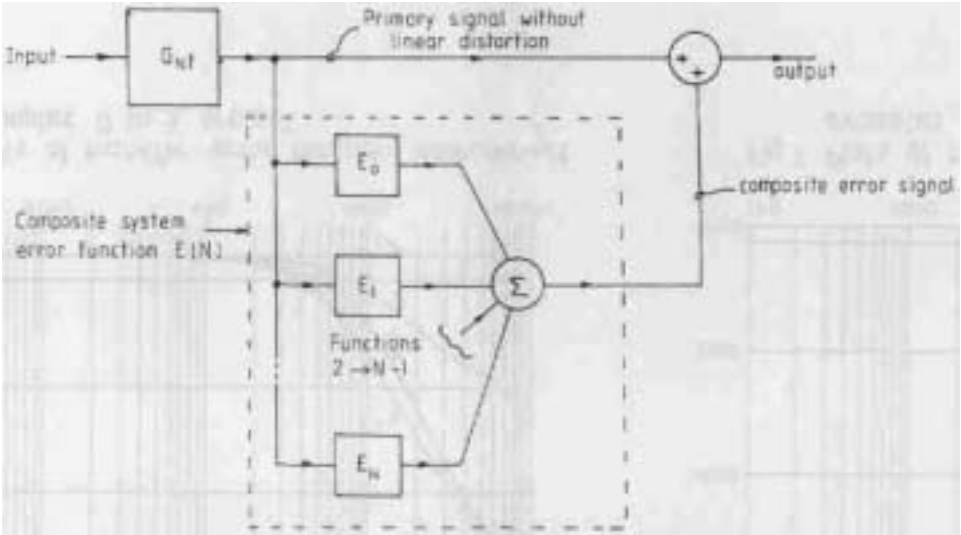

Fig. 5 Good approximation to the overall transfer-error function demonstrating individual errors are combined by addition NOT multiplication (ignoring error of error terms)

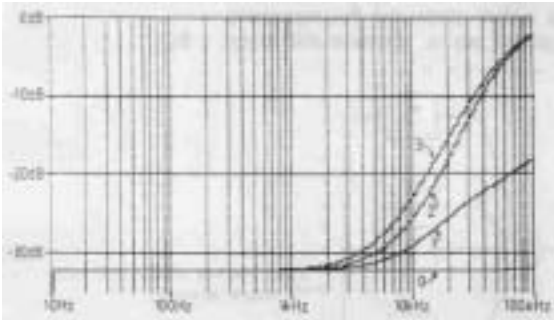

Fig 6 Plots of transfer-error function, interconnect examples 0 to 3, group 1

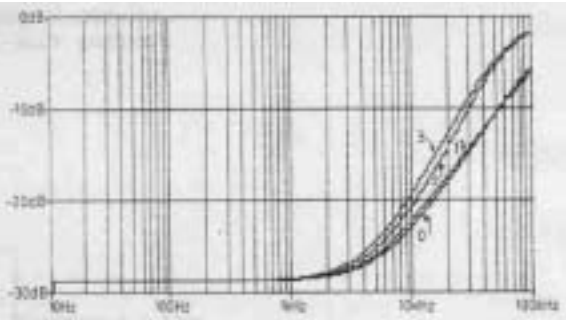

Fig 7 Plots of transfer-error function, interconnect examples 0 to 3, group 2

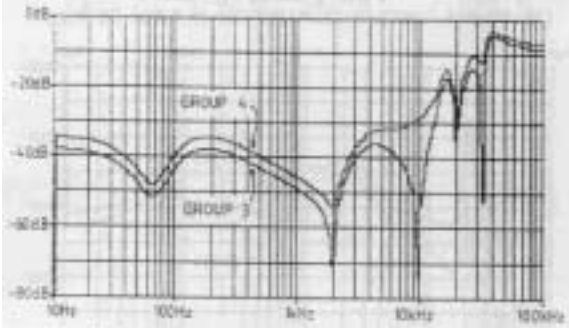

Fig 8a Plots of transfer-error function, interconnect example 0, group 3 and 4

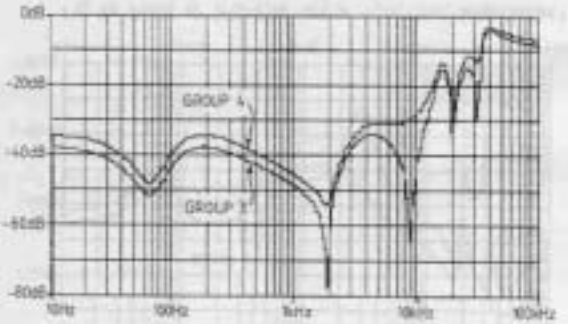

Fig 8b Plots of transfer-error function, interconnect example 1, group 3 and 4

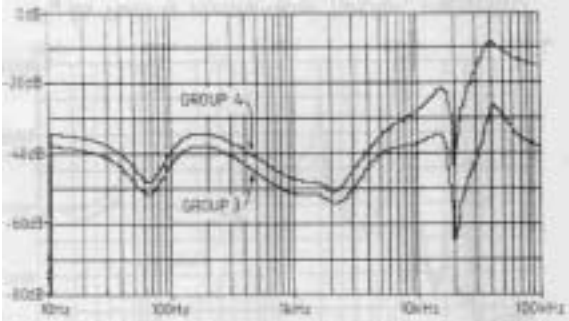

Fig 9a Plots of transfer-error function, interconnect example 2, groups 3 and 4

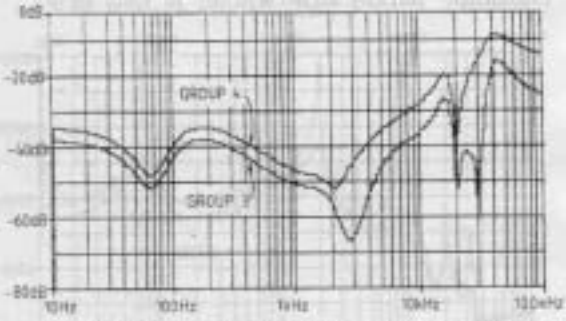

Fig 9b Plots of transfer-error function, interconnect example 3, groups 3 and 4

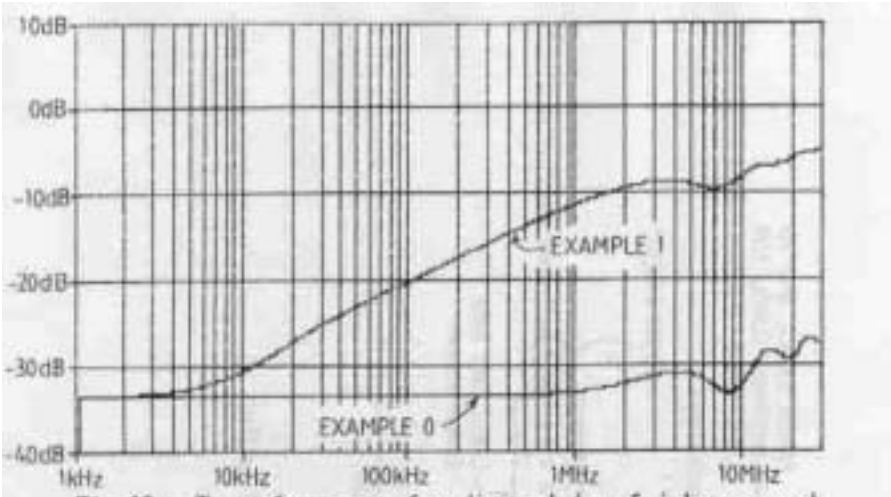

Fig. 10a Transfer-error function plots of interconnect examples 0 and 1, load impedance 4·712Ω// 0pF

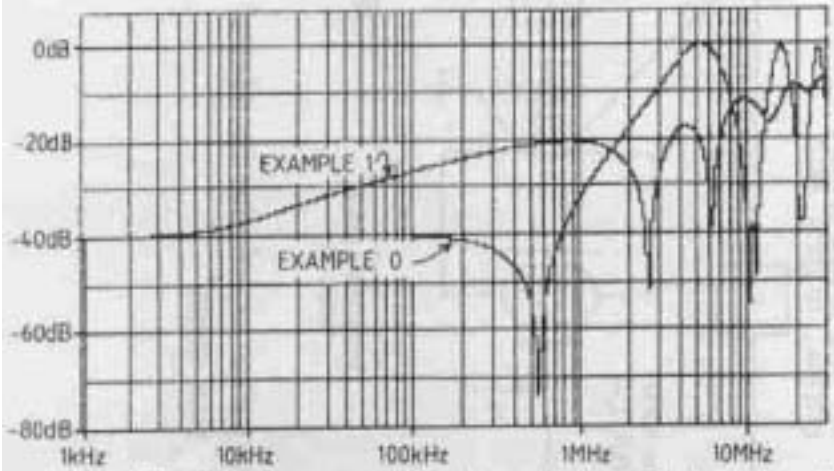

Fig. 10b Transfer-error function plots of interconnect examples 0 and 1, load impedance 10Ω// 0pF

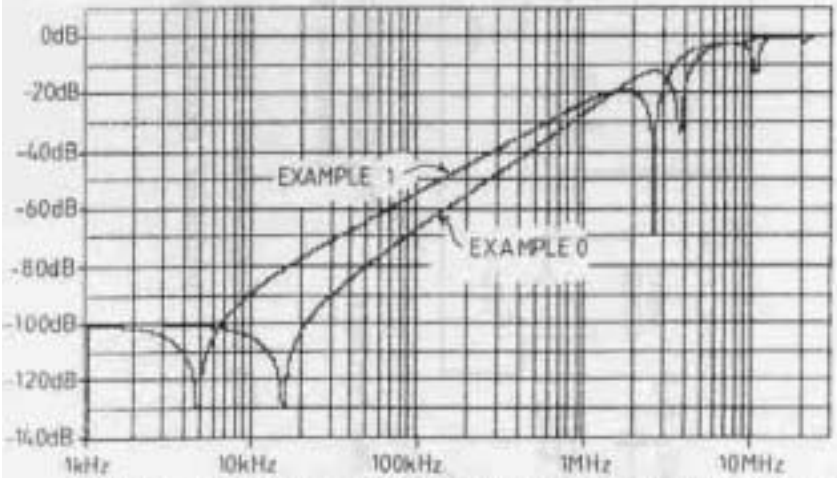

Fig. 10c Transfer-error function plots of interconnect examples 0 and 1, load impedance 10kΩ// 200pF

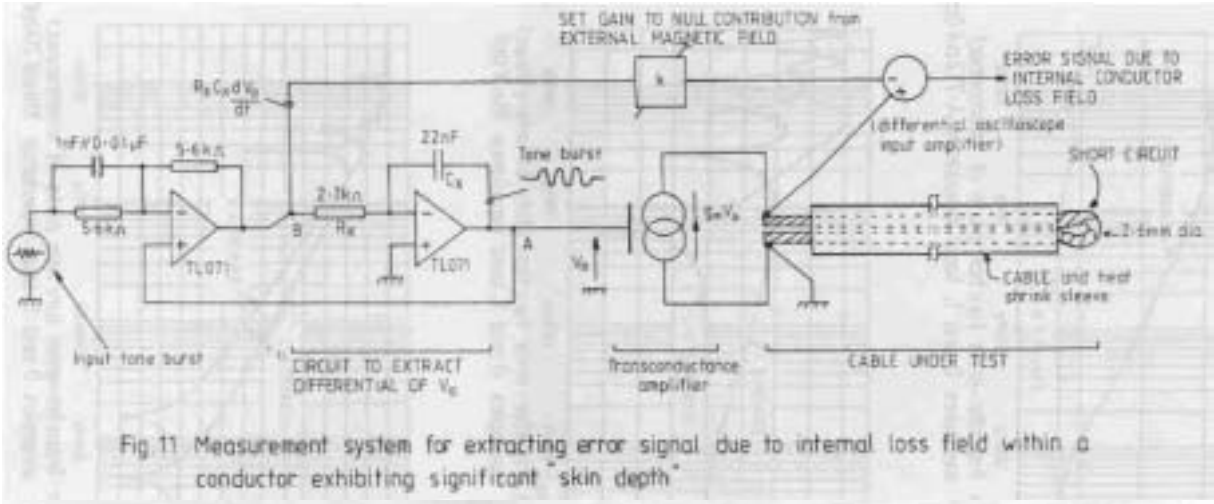

Fig.11 Measurement system for extracting error signal due to internal loss field within a conductor exhibiting significant "skin depth"

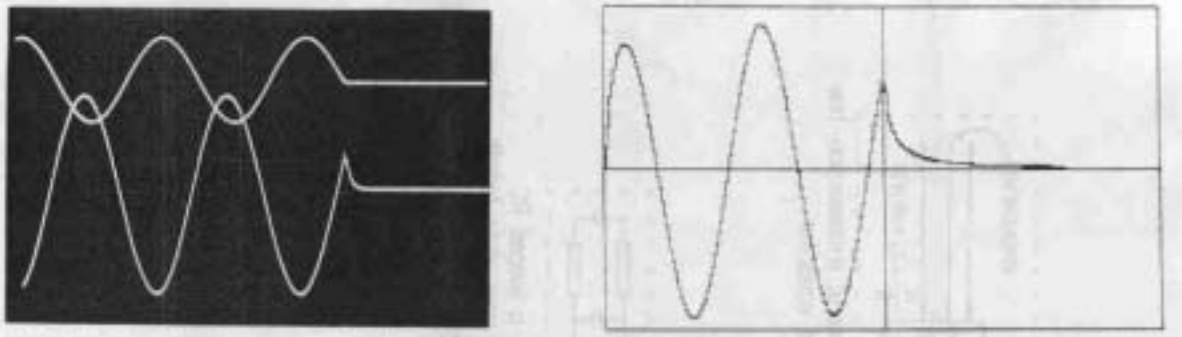

(a) Input tone-burst and measured output derived from system in Fig.11 representing error due to internal conductor fields

(b) Computer prediction of error due to internal conductor fields on tone-burst excitation

Fig.12 Computer prediction and measured responses of error due to internal loss field of conductor operating in skin-depth limited region (N.B. Input and output waveforms are NOT on same scale also time dispersion ∝ tone period in skin depth limited region, therefore time scale is immaterial)

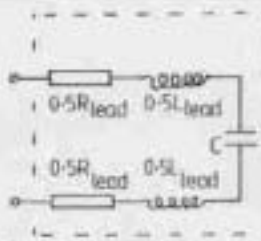

Fig. 13a Simple series RLC capacitor model

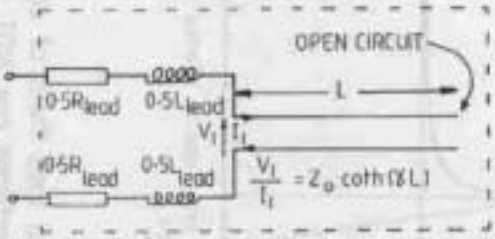

Fig. 13b More general transmission-line model of capacitor

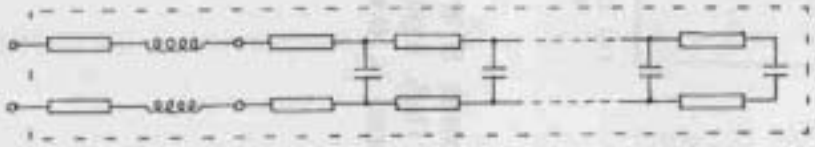

Fig. 13c Approximation to capacitor model using a lumped RC network to illustrate charge diffusion over plate length

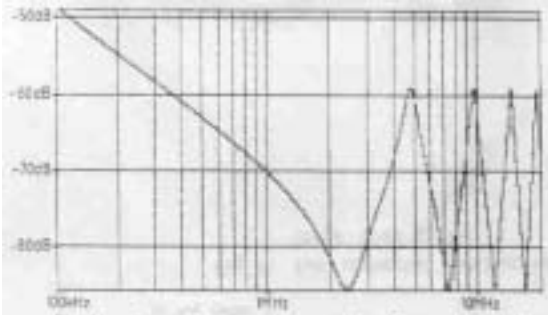

Fig. 14a Capacitor impedance plot, 10cm plate thickness (0dB ≡ 1Ω)

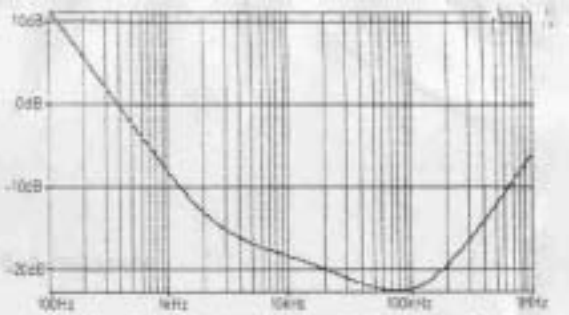

Fig. 14c Capacitor impedance plot including lead wire impedance (0dB ≡ 1Ω)

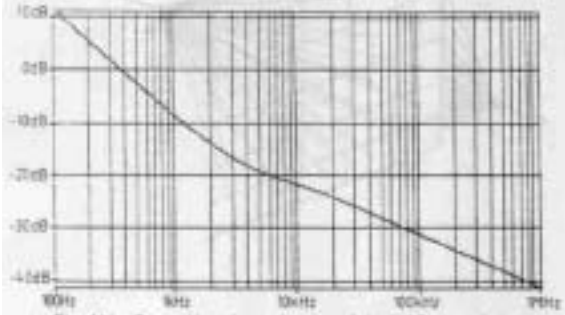

Fig. 14b Capacitor impedance plot, 0·05mm plate thickness (0dB ≡ 1Ω), lead wire impedance set to 0Ω

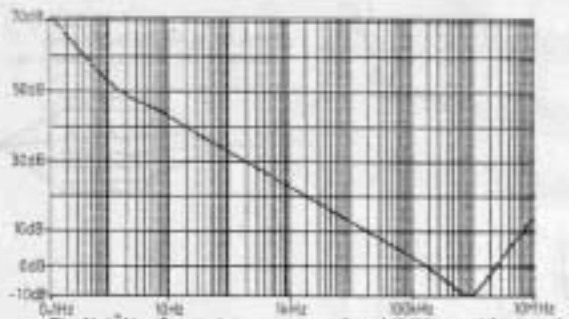

Fig. 14d "New" passive component exhibiting wide band -3dB/octave (-10dB/decade) impedance characteristic (0dB ≡ 1Ω)

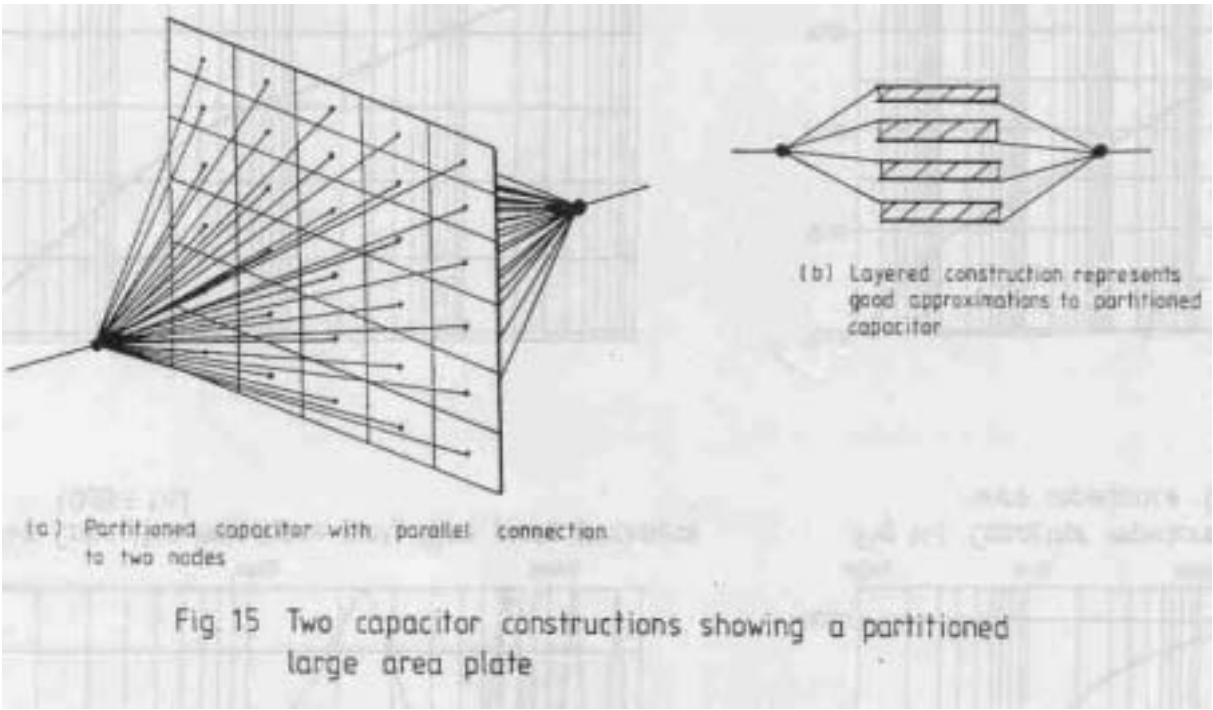

Fig. 15 Two capacitor constructions showing a partitioned large area plate

Appendix: Matlab program to explore different cable structures and plot both frequency and time domain responses

```
% Transmission line simulation program: translinecomp2_2.m   October 1999
% version 2.21
% Matlab 5.2 compliant
% compares a cable with resistance and skin effect with a line with no resistance and no skin effect
% effect BUT with the same shunt C series L, terminated in its characteristic impedance
% perform a time-domain input/output comparison for a tone burst, square wave, step and impulse bandlimited to bw
% 3 program types with individual data (refer to headings for data type)
% store program in directory "E:\matproj"
% create sub-directory "E:\matproj\Cable figures" to store figures

%
*****************************************************************************************************
% This propram uses a full transmission line model to calculate the transfer function of a cable.
% The model includes conductor skin depth, series inductance, shunt capacitance, series resistance and shunt resistance.
% A load impedance consisting of a shunt RC network is specified.
% The transfer function of an ideal cable (no resistance, no skin depth) terminated in its characteristic impedance is also calculated.
% The use of the ideal cable compensates for overall time delay.
% Results are represented as an error function which is the difference of the actual and idealised transfer functions.
% A result is also calculated on the basis the cables have zero skin effect, just pure resistance.
% Results are displayed in the frequency domain and in the time domain using a tone burst (an option for a full-wave rectified tone burst is included).
% Note that the cable resistance and skin depth effect mainly the low frequency characteristic impedance.
% At high frequency the external series L and shunt C dominate making the characteristic impedance almost resistive.
% Two cable options are included, rectangular conductors ie ribbon (2 versions) and cylindrical conductors.
% Cable parameters can be specified in the intro data to each cable type (keep a locked copy of the program for reference).
%
*****************************************************************************************************

% initialise program and select cable type
clear; close; home; clc; type=0; fwr=100; colordef black;
fprintf('TRANSMISSION LINE ANALYSIS PROGRAM\n\n\n')

% if prnt=1 save figures to file E:\matproj\Cable figures
fprintf('\nSave status for plots:\n');
prnt=input('Enter 1 to save to file, else 0:  ');

% select conductor type
fprintf('\n\nTYPE 1: rectangular conductors  DATA: width, thickness, spacing and resistivity\n')
fprintf('TYPE 2: cylindrical conductors  DATA: independent Rdc, L, C and conductor diameter\n')
fprintf('TYPE 3: cylindrical conductors  DATA: diameter, conductivity, series L shunt C deduced\n\n')
if type<4
type=input('Select "TYPE": 1, 2 or 3 (0 to terminate) '); type=round(abs(type));
if type==0
clc; home
return
end; end
home; clc

% Data entry
% ***************************************************************************************************
% TYPE 1: RIBBON CABLE DATA (DEFINE RIBBON GEOMETRY AND CONDUCTANCE)
if type==1
```

```
fprintf('Transmission-line ribbon-cable analysis program: calculate Rdc, L and C\n\n')
fprintf('Compares a cable with resistance and skin effect with a line with no resistance and no skin effect\n')
fprintf('BUT with the same shunt C series L ie nominal characteristic impedance\n\n')
fprintf('Tone-burst distortion displayed in time domain\n')

% data
% L      length of cable pair (metre)
% Rl     load resistance (ohm)
% Cl     load capacitance (farad)
% Ru                                    additional lumped dc resistance (ohm)
% Lu                                    additional lumped inductance (henry)
% Rp                                    cable shunt resistance/metre (ohm/metre)
% eps    permitivity of free space 8.855e-12 (farad/metre)
% epsr   relative permitivity
% mu                                    pemeability of free space (henry/metre)
% mur                                   relative pemeability
% rho                                   resistivity of conductor (ohm-centimetre)
% fmax                                  maximum display frequency (hertz)
% W                                     ribbon width (centi-metre)
% thk                                   ribbon thickness (centi-metre)
% delta  inter-ribbon space (milli-metre)
% stepf                                 number of displayed frequency steps
% fburst tone-burst frequency (herz)
% phi    tone-burst phase (degree)
% nc     number of cycles in tone burst
% bw     bandwidth of tone burst (hertz)
% rcb    raised-cosine transition band (hertz)

L=1.93;
Rl=2;
Cl=0*1e-12;
Ru=0;
Lu=0*1e-6;
Rp=10*1e6;
mu=4*pi*1e-7;
mur=1;
eps=8.855*1e-12;
epsr=2;
rho=3.21*1e-6;
fmax=1*1e6;
W=2.5;
thk=0.6;
delta=.05;
stepf=2^14;
fburst=1000;
phi=45;
nc=2;
bw=1*1e6;
rcb=2000;

% calculate static inductance/metre (Ls = 2*mu*delta/W)
eps=eps*epsr; mu=mu*mur; z=thk/2;
Ls=.2*mu*delta/W;

% calculate static capacitance/metre from Ls*Cp = eps*mu
Cp=eps*mu/Ls;

% calculate loop Rdc/metre
Rdc=2*rho*100/(W*thk);

% frequency steps
```

```
mm=1:stepf; fmin=fmax/stepf; rc=round(rcb/fmin);
f=fmin*mm;
w=2*pi*f;

% skin-depth parameters
skd=(100*rho*2./(mu*w)).^.5;
g=z*(1+i)./skd;

end
% ************************************************************************************************

% ************************************************************************************************
%TYPE 2: INDEPENDENT SELECTION OF SERIES INDUCTANCE, SHUNT CAPACITANCE AND DC RESISTANCE
% enter Ls, Cp and Rdc independently
if type==2
fprintf('Transmission-line cable analysis program: independent Rdc, L and C\n\n')
fprintf('Compares a line with resistance and skin effect with a line with no resistance and no skin effect\n')
fprintf('BUT with the same shunt C series L ie nominal characteristic impedance\n\n')
fprintf('Tone-burst and square-wave distortion displayed in time domain\n')

% data
% L      length of cable pair (metre)
% Rl     load resistance (ohm)
% Cl     load capacitance (farad)
% Ru                                    additional lumped dc resistance (ohm)
% Lu                                    additional lumped inductance (henry)
% Rdc    cable loop resistance/metre (ohm/metre)
% Ls                                    cable (external field) series inductance/metre (henry/metre)
% Cp                                    cable (external field) shunt capacitance/metre (farad/metre)
% Rp                                    cable shunt resistance/metre (ohm/metre)
% mu                                    pemeability of free space (henry/metre)
% mur                                   relative pemeability
% s                                     conductivity of conductor (ohm^-1)
% fmax                                  maximum display frequency (hertz)
% dia                                   conductor diameter (metre)
% stepf                                 number of displayed frequency steps
% fburst tone-burst frequency (herz)
% phi    tone-burst phase (degree)
% nc     number of cycles in burst
% bw     bandwidth of tone burst (hertz)
% rcb    raised-cosine transition band (hertz)

L=5;
Rl=10000;
Cl=200*1e-12;
Ru=0;
Lu=0*1e-6;
Rdc=10*1e-3;
Ls=22.5*1e-9;
Cp=1000*1e-12;
Rp=1*1e6;
mu=4*pi*1e-7;
mur=1;
s=5.8*1e7;
fmax=1*1e6;
dia=1*1e-3;
stepf=2^14;
fburst=4000;
phi=0;
nc=3.75;
```

```
bw=1*1e6;
rcb=2000;

% frequency steps
fmin=fmax/stepf;
mm=1:stepf; rc=round(rcb/fmin);
f=fmin*mm; mu=mu*mur; z=dia/2;
w=2*pi*f;

% skin-depth parameters
skd=(2./(mu*w*s)).^.5;
g=z*(1+i)./skd;

end
% ************************************************************************************************

% ************************************************************************************************
%TYPE 3: SELECT SERIES INDUCTANCE, PROGRAM CALCULATES SHUNT CAPACITANCE
if type==3
fprintf('Transmission-line cable analysis program: set L, calculate C and Rdc\n\n')
fprintf('Compares a line with resistance and skin effect with a line with no resistance and no skin effect\n')
fprintf('BUT with the same shunt C series L ie nominal characteristic impedance\n\n')
fprintf('Tone-burst distortion displayed in time domain\n')

% data
% L      length of cable pair (metre)
% Rl     load resistance (ohm)
% Cl     load capacitance (farad)
% Ru                                    additional lumped dc resistance (ohm)
% Lu                                    additional lumped inductance (henry)
% Ls                                    cable (external field) inductance/metre (henry/metre)
% Rp                                    cable shunt resistance/metre (ohm/metre)
% eps    permitivity of free space 8.855e-12 (farad/metre)
% epsr   relative permitivity
% mu                                    pemeability of free space (henry/metre)
% mur                                   relative pemeability
% s                                     conductivity of conductor (ohm^-1)
% fmax                                  maximum display frequency (hertz)
% dia                                   conductor diameter (metre)
% stepf                                 number of displayed frequency steps
% fburst tone-burst frequency (herz)
% phi    tone-burst phase (degree)
% nc     number of cycles in burst
% bw     bandwidth of tone burst (hertz)
% rcb    raised-cosine transition band (hertz)

L=5;
Rl=2.9978;
Cl=1000*1e-12;
Ru=.01;
Lu=.01*1e-6;
Ls=.01*1e-6;
Rp=1*1e6;
mu=4*pi*1e-7;
mur=1;
eps=8.855*1e-12;
epsr=2;
s=5.8*1e7;
fmax=1*1e6;
dia=2*1e-3;
stepf=2^14;
```

```
fburst=4000;
phi=0;
nc=3.75;
bw=1*1e6;
rcb=2000;

% calculate capacitance from Ls*Cp = eps*mu
eps=eps*epsr; mu=mu*mur; z=dia/2;
Cp=eps*mu/Ls;

% calculate loop resistance/metre Rdc
Rdc=2/(s*pi*z^2);

% frequency steps
mm=1:stepf; fmin=fmax/stepf; rc=round(rcb/fmin);
f=fmin*mm;
w=2*pi*f;

% skin-depth parameters
skd=(2./(mu*w*s)).^.5;
g=z*(1+i)./skd;

end
% ********************************************************************************************
% END OF DATA ENTRY


% MAIN PROGRAM

fprintf('\n\nCOMPUTING: frequency domain\n\n')

% auto set tone-burst frequency fburst comensurate with fmax
dis=0;
if fburst/fmin<3*nc
fburst=3*nc*fmin;
dis=1;
end
kf=ceil(fburst/fmin);
steps=2*stepf; phi=phi*pi/180;
ft=kf/steps; ss=round(nc*steps/kf);
soff=ss;
bww=floor(abs(bw/fmin));

% start frequency-domain analysis

% cable transfer function "at" is calculated as a 3 row matrix
% row1: all series parameters (R, L and skin depth effect) including skin depth. load impedance is shunt RC
% row2: series parameters as row 1 but excluding skin depth. load impedance is shunt RC
% row3: series L only, no resistive loss or skin depth. load impedance = characteristic impedance

% calculate load impedance (parallel Rl//Cl) zzl
char=(Ls/Cp)^.5;
zzl(1,mm)=Rl*ones(size(mm))./(1+i*w*Rl*Cl);
zzl(2,mm)=Rl*ones(size(mm))./(1+i*w*Rl*Cl);
%zzl(3,mm)=Rl*ones(size(mm))./(1+i*w*Rl*Cl);
zzl(3,mm)=char*ones(size(mm));

% calculate source impedance of generator zs
zs(1,mm)=Ru*ones(size(mm))+i*w*Lu;
zs(2,mm)=Ru*ones(size(mm))+i*w*Lu;
zs(3,mm)=Ru*ones(size(mm))+i*w*Lu;
```

```
% calculate cable shunt impedance parameters c + jd
cd(1,mm)=(Rp^-1)+i*(w*Cp);
cd(2,mm)=(Rp^-1)+i*(w*Cp);
cd(3,mm)=i*(w*Cp);

% calculate cable series impedance parameters a + jb
ab(1,mm)=Rdc*g.*coth(g)+i*w*Ls;
ab(2,mm)=Rdc+i*w*Ls;
ab(3,mm)=1e-10*i*w*Ls;

% calculate cable propagation constant gam
gam=[ab.*cd].^.5;

% calculate cable characteristic impedance zo
zo=[ab./cd].^.5;

% calculate input impedance zin of cable and load
zin=zo.*((zzl.*cosh(gam*L)+zo.*sinh(gam*L))./(zzl.*sinh(gam*L)+zo.*cosh(gam*L)));

% calculate overall transfer function "at" of cable including source impedance
at=((1+zs./zzl).*cosh(gam*L)+(zo./zzl+zs./zo).*sinh(gam*L)).^-1;
at=[at conj(at(1:3,stepf:-1:1))];

% calculate transfer-error function err (cable tf loaded with zzl - idealsed cable tf loaded with zo)
err(1,mm)=-at(1,mm)+at(3,mm);
err(2,mm)=-at(2,mm)+at(3,mm);
err=[err conj(err(1:2,stepf:-1:1))];

% plot frequency domain error functions
semilogx(f,20*log10(abs(err(1,mm))),'r')
hold on; grid
semilogx(f,20*log10(abs(err(2,mm))),'b')
title('Error function against perfect matched line dB/log(freq): red with skin effect, blue no skin effect')
if prnt==1
print -dbitmap E:\matproj\Cable figures\Figure1-1
end;
pause; close
semilogx(f,abs(zin(1,mm)),'r')
hold on; grid
semilogx(f,abs(zin(2,mm)),'b')
title('Modulus of cable input impedance: red with skin effect, blue without skin effect')
if prnt==1
print -dbitmap E:\matproj\Cable figures\Figure1-2
end;
pause; close

% plot frequency domain transfer functions
semilogx(f,20*log10(abs(at(1,mm))),'r')
hold on; grid
semilogx(f,20*log10(abs(at(2,mm))),'b')
semilogx(f,20*log10(abs(at(3,mm))),'g')
title('Transfer function dB/log(freq): red with skin effect (load R//C), blue no skin effect (load R//C), green
lossless (load charcteristic impedance)')
if prnt==1
print -dbitmap E:\matproj\Cable figures\Figure1-3
end;
pause; close

% end frequency-domain analysis
% ************************************
```

```
% start time-domain analysis for sine/square tone burst

% calculate tone burst and corresponding fourier transform
% select normal, full-wave rectified tone burst or square-wave
while fwr>4
fwr=input('Select gated waveform: 0 sine, 1 full-wave sine rectified, 2 square-wave, 3 step response, 4 impulse response: '); fwr=round(abs(fwr));
end
if fwr==1
fwro=1;
else
fwro=0;
end
lpf=[ones(size(1:bww-rc)) .5*(1+cos(pi*(1:rc)/rc))];
bww=[lpf(1:bww) zeros(size(bww+1:steps-bww)) lpf(bww:-1:1)];
tone=(1-fwro)*[zeros(size(0:soff-1)) sin(2*pi*ft*(0:ss-1)+phi) zeros(size(ss:steps-soff-1))];
tone=tone+fwro*[zeros(size(0:soff-1)) abs(sin(2*pi*ft*(0:ss-1)+phi)) zeros(size(ss:steps-soff-1))];
if fwr==2
tone=sign(tone);
end
if fwr==3
tone=[zeros(size(0:soff-1)) ones(size(0:ss-1)) ones(size(ss:steps-soff-1))];
end
if fwr==4
tone=zeros(size(1:steps));
tone(soff)=1;
end
fprintf('\n\nCOMPUTING: time domain\n\n')
bs=size(bww);
bt=size(tone);
if bs(2)>bt(2)
fprintf('\n\nTone bandwidth bw too large, defaulting to bw = \n')
stepf*fmin
tfreq=fft(tone);
else
tfreq=fft(tone).*bww;
end
toneb=real(ifft(tfreq));

% calculate time domain error with and without skin depth effect
errt(1,1:steps)=real(ifft(tfreq.*err(1,1:steps)));
errt(2,1:steps)=real(ifft(tfreq.*err(2,1:steps)));

% calculate time domain output with and without skin depth effect
outt(1,1:steps)=real(ifft(tfreq.*at(1,1:steps)));
outt(2,1:steps)=real(ifft(tfreq.*at(2,1:steps)));

% auto-scaling time domain plot range in micro second
if fwr<3
su=round(2.25*ss); sl=round(.75*ss);
else
sl=round(ss);
su=sl+10;
while abs(errt(1,su))>.2*max(abs(errt(1,1:steps)))
su=su+1;
end; end
ts=(0:su-sl)*10^6/(steps*fmin);

% plot time domain error waveforms
```

```
plot(ts,max(abs(errt(1,sl:su)))*toneb(sl:su),'g')
hold on
plot(ts,errt(1,sl:su),'r')
title('Time-domain error (micro-s): red with skin effect | green input (input not to scale)')
if prnt==1
print -dbitmap E:\matproj\Cable figures\Figure2-1
end;
pause; close
plot(ts,max(abs(errt(2,sl:su)))*toneb(sl:su),'g')
hold on
plot(ts,errt(2,sl:su),'b')
title('Time-domain error (micro-s): blue no skin effect | green input (input not to scale)')
if prnt==1
print -dbitmap E:\matproj\Cable figures\Figure2-2
end;
pause; close
plot(ts,max(abs(errt(1,sl:su)))*toneb(sl:su),'g')
hold on
plot(ts,errt(1,sl:su),'r')
plot(ts,errt(2,sl:su),'b')
title('Superimposed errors (micro-s): red skin effect | blue no skin effect | green input (input not to scale)')
if prnt==1
print -dbitmap E:\matproj\Cable figures\Figure2-3
end;
pause; close; clc
if dis==1
fprintf('NOTE: fburst re-scaled\n')
fburst
end

% plot time domain output waveforms
plot(ts,toneb(sl:su),'g')
hold on
plot(ts,outt(1,sl:su),'b')
plot(ts,toneb(sl:su)-outt(1,sl:su),'r')
title('Time-domain (micro-s): green input | blue output with skin effect | red (input - output) error')
if prnt==1
print -dbitmap E:\matproj\Cable figures\Figure2-4
end;
pause; close
plot(ts,toneb(sl:su),'g')
hold on
plot(ts,outt(2,sl:su),'b')
plot(ts,outt(2,sl:su)-outt(2,sl:su),'r')
title('Time-domain (micro-s): green input | blue output no skin effect | red (input - output) error')
if prnt==1
print -dbitmap E:\matproj\Cable figures\Figure2-5
end;
pause; close
if dis==1
fprintf('NOTE: fburst re-scaled\n')
fburst
end

% end time-domain analysis

return
% ************************************************
```